

2 Experimental Characterization Techniques

Chapter Outline

2.1	Introduction	20
2.2	Mechanical Testing for Material Model Calibration	22
2.2.1	Uniaxial Compression Testing	24
2.2.2	Uniaxial Tension Testing	29
2.2.3	Plane Strain Tension	33
2.2.4	Simple Shear Testing	37
2.2.5	Impact Testing	40
2.2.6	Dynamic Mechanical Analysis	43
2.2.7	Hardness and Indentation Testing	47
	Rockwell Hardness Testing	47
	Shore (Durometer) Testing	48
	Barcol Hardness Testing	50
	Nanoindentation	51
2.2.8	Split-Hopkinson Pressure Bar Testing	53
2.2.9	Bulk Modulus Testing	64
2.2.10	Other Common Mechanical Testing Modes	71
2.2.11	Testing for Failure Model Calibration	73
2.3	Mechanical Testing for Material Model Validation	73
2.3.1	Material Model Verification and Validation	75
2.3.2	Small Punch Testing	77
2.3.3	V-Notch Shear Testing	80
2.4	Surface Characterization Techniques	80
2.4.1	Optical Microscopy	81
2.4.2	Scanning Electron Microscopy	84
2.4.3	Atomic Force Microscopy	87
2.5	Volume Characterization Techniques	89
2.5.1	Differential Scanning Calorimetry	89
2.5.2	Transmission Electron Microscopy	90
2.5.3	X-Ray Diffraction	92

Wide-Angle X-Ray Diffraction	93
Small-Angle X-Ray Diffraction	95
2.5.4 Birefringence	95
2.5.5 Swell Testing	97
2.6 Chemical Characterization Techniques	99
2.6.1 Fourier Transform Infrared Spectroscopy	100
2.6.2 Energy Dispersive Spectroscopy	101
2.6.3 Size-Exclusion Chromatography	103
2.6.4 Thermogravimetric Analysis	107
2.6.5 Raman Spectroscopy	109
2.7 Exercises	110
References	112

2.1 Introduction

One of the key components of polymer mechanics is experimental material characterization. Polymers, due to their macromolecular structure, exhibit not only a wide range of different behaviors but also rapid changes in behavior for limited variations in load environment and temperature. At low temperatures (relative to the glass transition temperature), polymers behave as stiff solids that if deformed enough start to undergo viscoplastic deformation. At temperatures in the vicinity of the glass transition temperature, polymers typically exhibit a leathery or rubbery response. At high temperatures, above both the glass transition temperature and the melting temperature, the response is viscous and liquid-like if the polymer is uncrosslinked, rubbery if the material is weakly crosslinked, and stiff viscoelastic if the material is highly crosslinked. It is important to understand and be able to experimentally determine these characteristic behaviors, and this is the topic of [Section 2.2](#) of this chapter.

Experimental testing can be performed for different reasons. One common reason is to obtain enough information to calibrate one or more material models. Another reason is to obtain information related to when and how a material fails; that is, to obtain information for failure model calibration. Sometimes testing is also performed for quality control purposes, or to characterize

certain aspects of the material response or structure. The focus of this chapter is on experimental testing for material model and failure model calibration, and also on validating already calibrated models. There is an almost unlimited amount of different testing techniques that are available for this purpose, and this chapter is simply focused on presenting some of the more commonly used and some of the most useful methods.

An experimental test program for material model calibration typically consists of multiple individual experiments, each of which is performed in a specific loading mode, with a specific applied stress/strain load history, in a given temperature environment. [Figure 2.1](#) shows a schematic representation of an experimental test program and how it connects to finite element (FE)

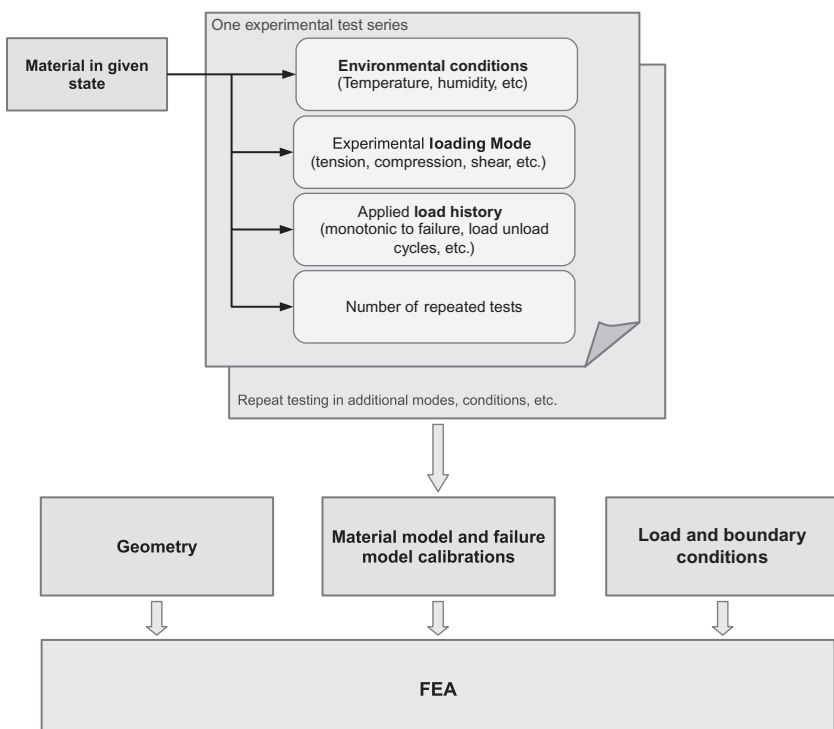


Figure 2.1 An experimental testing program consists of multiple individual experiments each of which needs the specification of the loading mode, the applied load history, the environmental conditions, and the number of repeated tests.

investigations. Much of the materials covered in this chapter are targeted to how to properly design an experimental test program for the purpose of material model calibration and validation.

Another aspect of polymer characterization is related to the *morphology* of the material, either for a surface or for the bulk volume. Experimental techniques designed for this purpose are discussed in [Sections 2.4](#) and [2.5](#), respectively. The goal of these experimental characterization techniques is to probe or investigate different aspects of the microstructure of the material. For example, the presence of microcracks, the degree of crystallinity, and the type of crystal structure can all be examined using these techniques.

The last section of this chapter ([Section 2.6](#)) discusses chemical characterization techniques that are useful for polymers. The results from these techniques are not useful for phenomenological polymer mechanics modeling, but can be very useful and informative in experimental studies of for example fatigue, and material degradation. These chemical characterization techniques are also immensely important in polymer failure analysis. When faced with mechanical failure or fracture of a polymer product, one of the first investigations that is often done is to make sure the polymer that was used in the product was of the right type, and that the molecular structure of the polymer was what it was supposed to be. The chemical characterization techniques can answer these questions. The information obtained through chemical characterization can also be used to better understand the mechanical behavior of polymers on a microlevel, and as will be discussed in Chapter 8, is useful for developing micromechanical models.

2.2 Mechanical Testing for Material Model Calibration

The most common method to experimentally characterize the mechanical response of a polymer involve mechanically loading a polymer component or test specimen, and measuring the resulting force and displacement response. There are many different ways

this can be performed. This section summarizes some of the more common experimental characterization techniques.

One of the most basic mechanical tests—perhaps even the most important polymer mechanics test—is a test designed to determine the stress-strain response of a given polymer. The stress-strain response will dictate the deformation characteristics of the polymer in its intended application, and is therefore a key component for quantifying not only the deformation behavior but also fatigue and fracture resistance. As discussed above, one complication for polymers is that the stress response during an imposed deformation history is strongly dependent on the material, the applied rate of deformation, and the temperature. These factors all play an important role when designing or choosing a mechanical test for polymers. The influence of temperature, in particular, has utmost influence on all aspects of the mechanical response of polymers. One way this is often presented is in terms of the dependence of the material stiffness (Young's modulus) on the temperature, see [Figure 2.2](#).

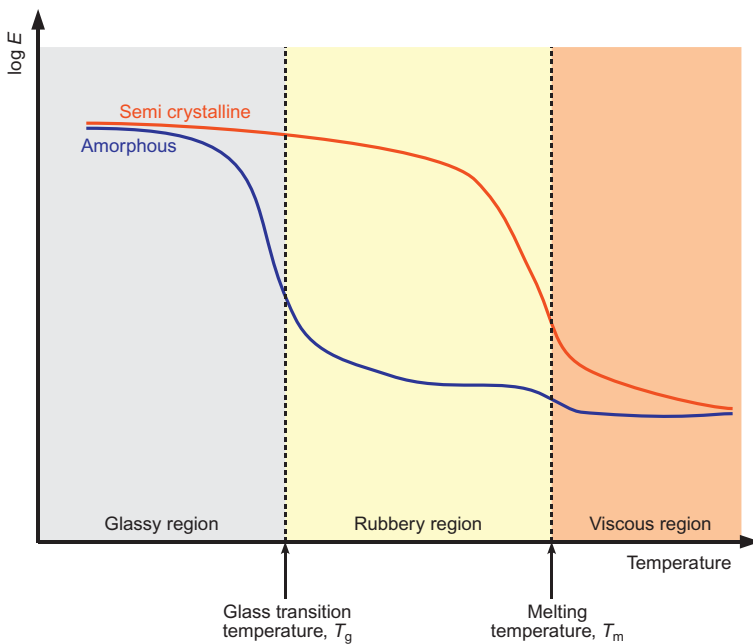


Figure 2.2 Dependence of the Young's modulus on the temperature for different classes of polymers.

For example, the glass transition temperature for PET is about 70 °C (343 K) and the melting temperature is about 250 °C (523 K), so at room temperature this polymer will already be at 85% of its glass transition temperature, and 56% of its melting temperature. The thermal activation barrier to viscoelastic and viscoplastic flow is therefore small in many normal applications, resulting in a complicated macroscopic response when exposed to external loads.

In a broad sense, the stress-strain response of polymers can be divided into three different categories, each with its own distinct features: (1) deformation of elastomers and thermoplastic elastomers (TPE); (2) deformation of thermoplastics below the glass transition temperature; and (3) deformation of highly crosslinked thermosets. Characteristic experimental features of these different categories are illustrated in [Figures 2.3, 2.4](#), and [2.5](#), respectively.

2.2.1 Uniaxial Compression Testing

The most common method to experimentally determine the stress-strain response of a material is to perform uniaxial tension or compression tests. In these tests, the test specimen is loaded in a designated test machine using grips for tension tests, and compression platens for compression tests. The specimen deformation is typically measured using an extensometer or strain gauge, either contacting the specimen or by using optical techniques.

Both uniaxial tension and uniaxial compression tests have strengths and limitations. For the uniaxial compression tests, the interface friction between the test specimen and the loading platens can cause a nonhomogeneous deformation state, often indicated by barreling of the test specimen, see [Figure 2.6](#).

This figure shows FE predictions of both the deformed shape and the change in the measured engineering stress as a function of the friction coefficient and the applied strain. The initial diameter of the test specimen that was used in the virtual experiments was 28.6 mm and the initial height was 12.5 mm. These values follow the recommendations in ASTM D575 [1]. A Neo-Hookean

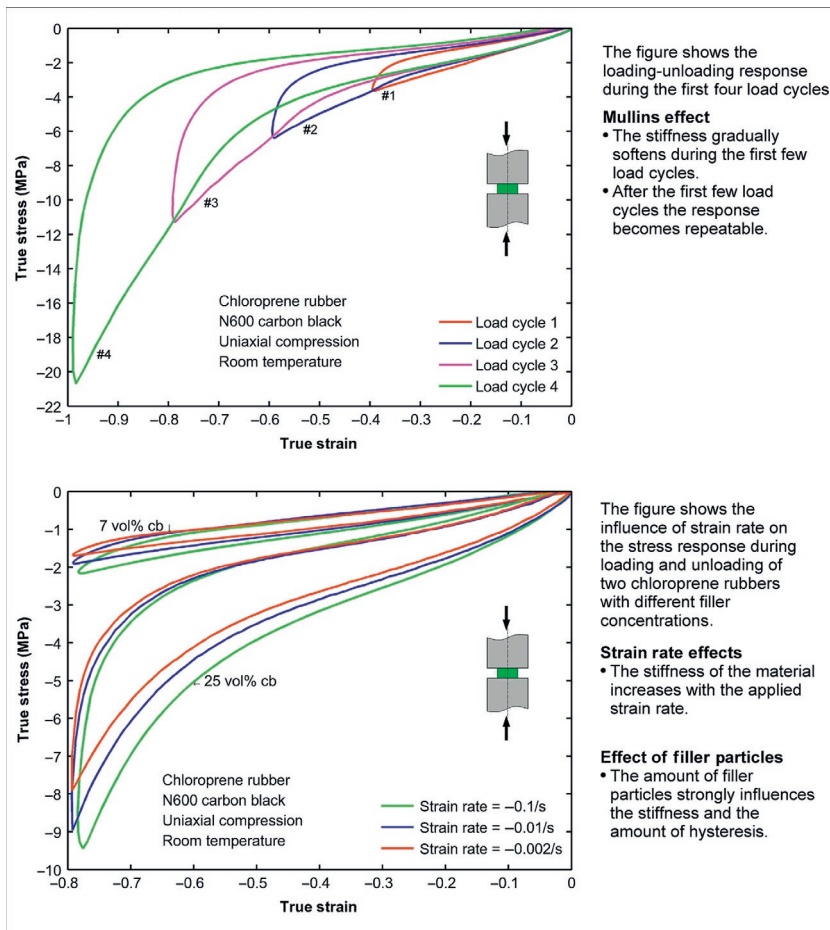


Figure 2.3 Characteristic stress-strain response of elastomers loaded above the glass transition temperature.

material model with a shear modulus of 2 MPa and a bulk modulus of 200 MPa was used to represent the polymer. The results clearly show that significant barreling can occur even when the friction coefficient is as low as 0.1, and the error in the stress is not trivial for finite strains.

The error in the stress predictions can be obtained by comparing the results from the case with friction to the case without friction. The relative error in the predictions from this test case is plotted in Figure 2.7 showing that the error is almost linearly

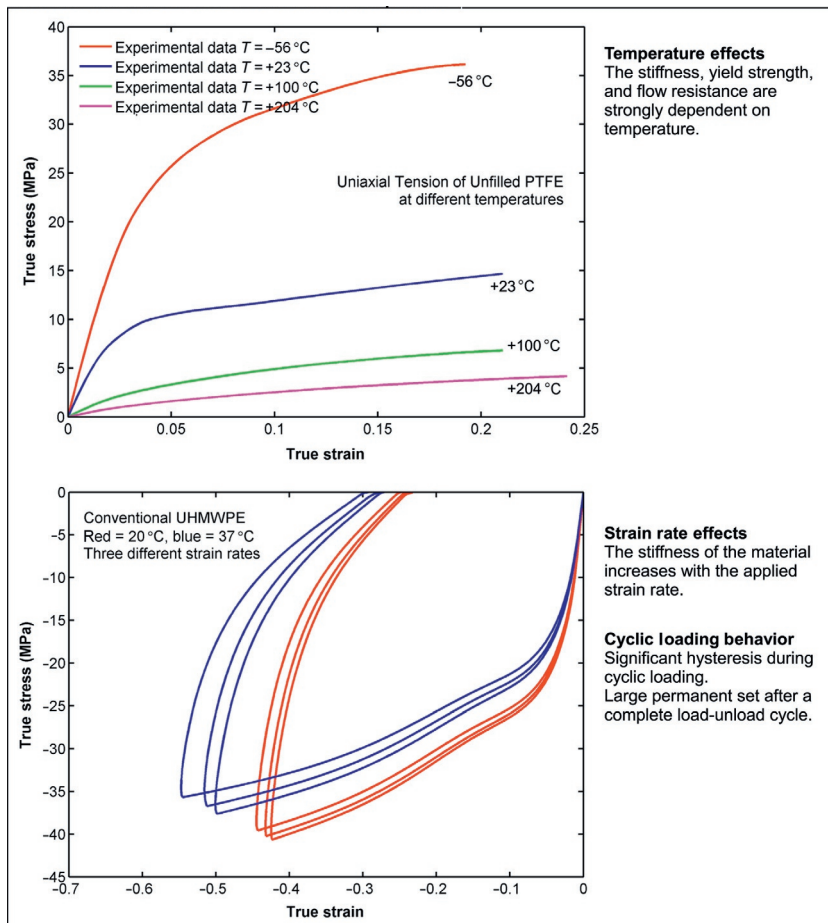


Figure 2.4 Characteristic stress-strain response of thermoplastics below the glass transition temperature.

depend on the friction coefficient and weakly dependent on the applied strain.

The stress and strain inside the test specimen becomes inhomogeneous when there is a nonzero friction coefficient. As an example, [Figure 2.8](#) shows a cut through a specimen with a diameter of 28.6 mm and a height of 12.5 mm (Following ASTM D575 [1]) that was compressed to an engineering strain of -0.3 with a friction coefficient of 0.1. In this case, the max Mises stress is about 4.5 times higher than the lowest Mises stress, which is quite substantial.

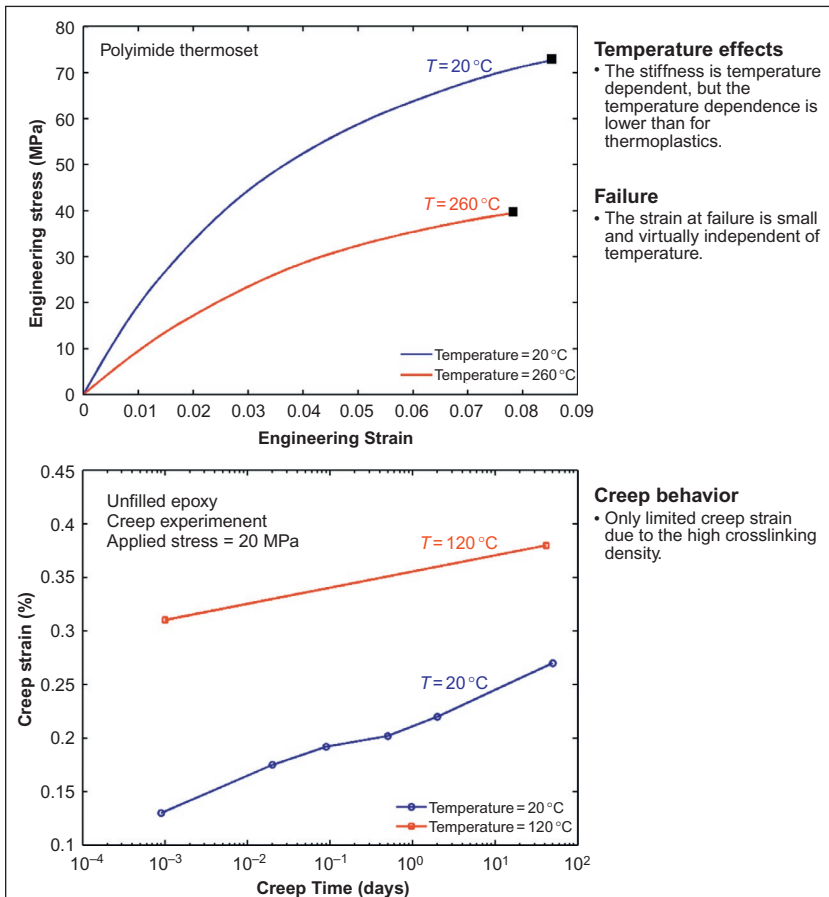


Figure 2.5 Characteristic stress-strain behavior of thermosets.

One way to reduce the influence of the interface friction is to make the specimen height/diameter ratio larger. Figure 2.9 shows the results from virtual experiments of specimens with different heights but the same diameter. In this case, the relative error in the stress measurement goes down from 11.5% to 3.5%, at an applied strain of -0.2, if the specimen height to diameter ratio increases from 0.44 to 1.31. It is important, however, not to make the test specimen too tall since that can cause a buckling instability during the compression testing.

Interface friction in a compression experiment influences not only the stiffness during monotonic loading but also the stress

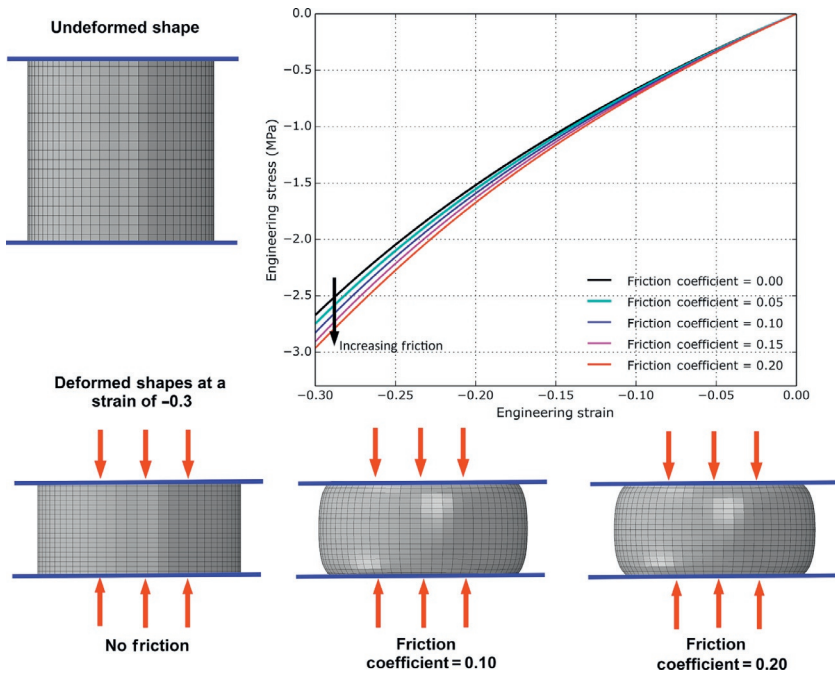


Figure 2.6 3D FE results showing the influence of interface friction on the deformed specimen shape and the stress-strain response. The polymer was modeled using a Neo-Hookean material model with a shear modulus of 2.0 MPa and a bulk modulus of 20.0 MPa.

response during unloading. This effect especially changes the response during the initial unloading part of an experiment. This behavior is examined using FE-based virtual experiments summarized in Figure 2.10. As shown in the figure, a simple hyperelastic Neo-Hookean material dissipates energy during cyclic loading when there is interface friction, and a nonlinear viscoelastic material, here represented using the Bergstrom-Boyce (BB) model, changes its behavior during the loading phase and during the initial part of the unloading. The frictional effects specifically increase the slope of the stress-strain curve right after unloading. This behavior is easy to misinterpret as an indication of a Mullins (or other) damage mechanism, but can simply be a consequence of the interface friction.

To reduce the amount of barreling it is common to lubricate the interface between the specimen and the loading platens,

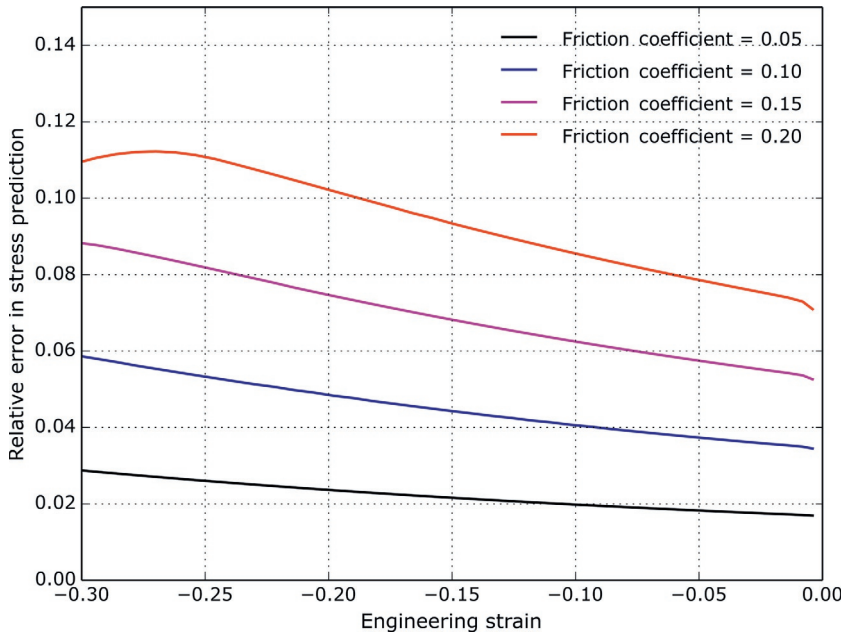


Figure 2.7 FE results showing the influence of interface friction on the predicted error in the measurement results. The polymer was modeled using a Neo-Hookean material model with a shear modulus of 2.0 MPa and a bulk modulus of 20.0 MPa.

for example by a nonaggressive oil or liquid soap [2]. Another alternative is to use PTFE sheets at the interfaces [2, 3].

If the purpose of the experimental testing is to obtain suitable experimental data for material model calibration, then it is still possible to use compression data as long as the friction coefficient is known or can be estimated. In this case, the material model calibration is best performed using FE simulations of the actual experiments that were formed. This topic is discussed in more detail in Chapter 9.

2.2.2 Uniaxial Tension Testing

In uniaxial tension testing, the loading grips will always introduce stress concentrations in the part of the specimen that is close to the gripped regions. To reduce the influence of these stresses the test specimens are typically given a dog-bone shape.

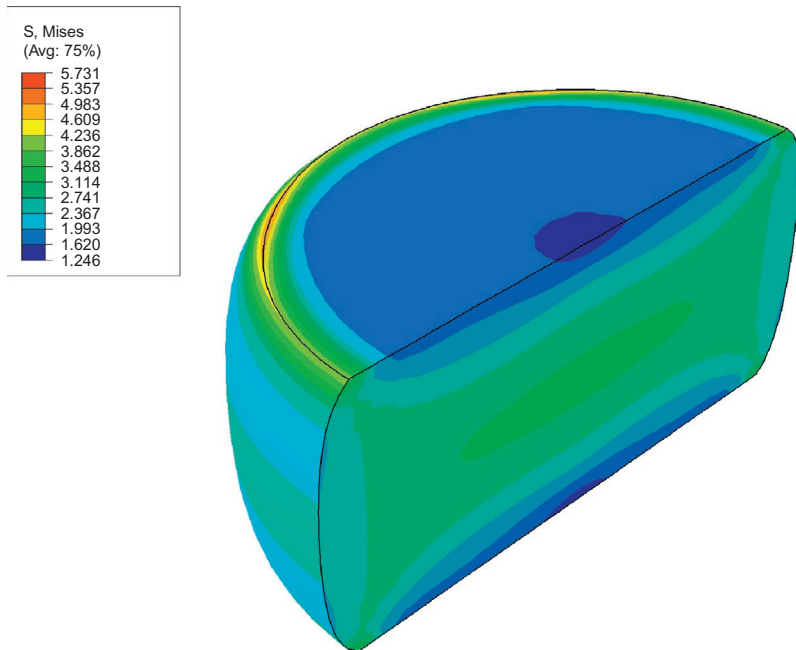


Figure 2.8 Predicted contours of Mises stress. The polymer was modeled using a Neo-Hookean material model with a shear modulus of 2.0 MPa and a bulk modulus of 20.0 MPa. Applied engineering strain = -0.3 , friction coefficient = 0.1.

This specimen design will create an almost uniform uniaxial deformation and stress state in the central gauge region of the specimen. Details of recommended test specimen geometries are given in different standards [4–6]. Figure 2.11 shows the distribution of Mises stress in an ASTM D638 Type IV specimen pulled in tension to a true strain of approximately 15%. In this case, the test specimen was represented using a Neo-Hookean material model with a shear modulus of 2 MPa and a bulk modulus of 200 MPa. The green region in the figure has a stress that is varying less than 1%.

One complication that can occur with dog-bone shaped specimen during tensile loading is *necking*. This is a phenomenon that is important to be aware of since it creates an inhomogeneous deformation state in the specimen, and hence makes it difficult to extract the actual stress-strain response unless the localized deformation state is directly measured using, for example, digital

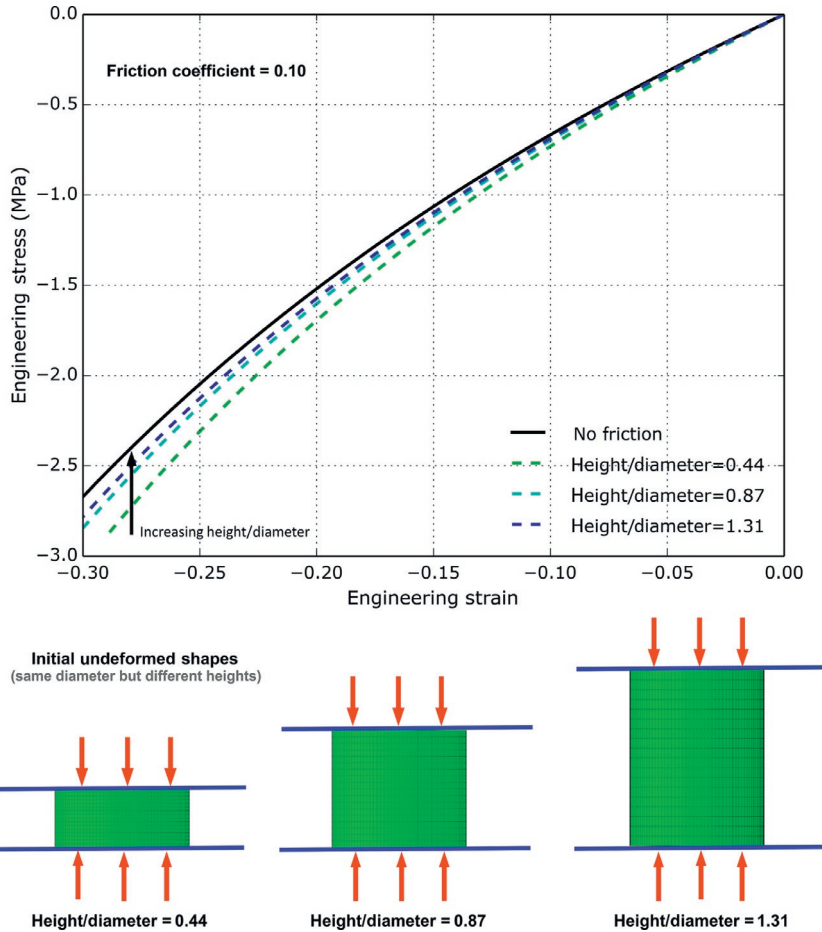


Figure 2.9 FE results showing the influence of specimen height to diameter ratio on the measurement results. The polymer was modeled using a Neo-Hookean material model with a shear modulus of 2.0 MPa and a bulk modulus of 20.0 MPa.

image correlation. The mathematical details of necking are given in [Figure 2.12](#). As is shown in this figure the traditional condition for necking is the following:

$$\frac{d\sigma^{\text{eng}}}{d\varepsilon^{\text{eng}}} = 0. \quad (2.1)$$

That is, if there is a peak in the engineering stress versus engineering strain curve then the specimen may neck. In practice,

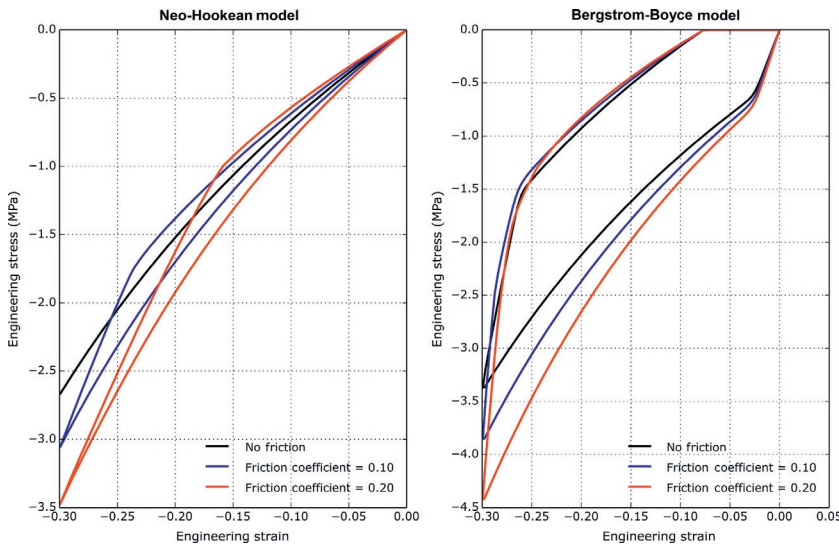


Figure 2.10 FE results showing the influence of interface friction on the predicted stress-strain response during both loading and unloading. The frictional forces influence both the tension and the compression responses.

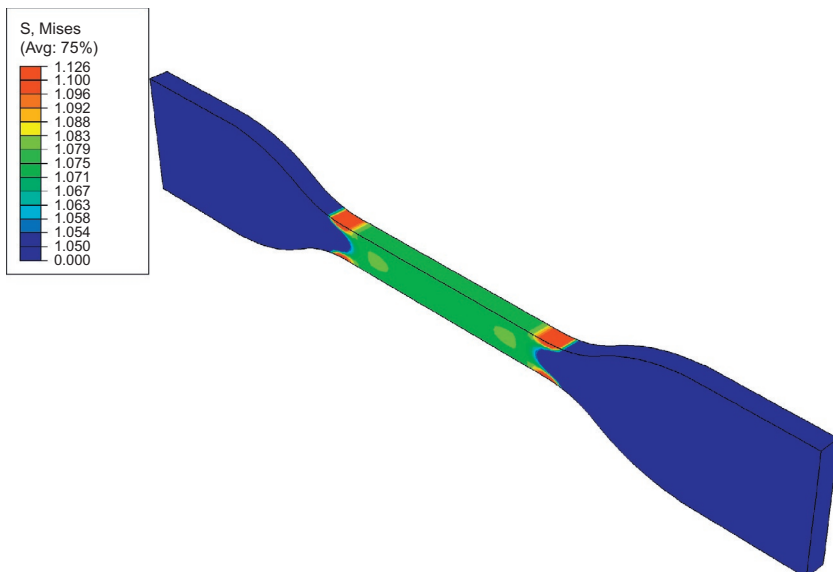


Figure 2.11 Stress distribution inside an ASTM D638 Type IV specimen pulled in tension to a true strain of about 15%. The material was represented using a Neo-Hookean material model with a shear modulus of 2.0 MPa and a bulk modulus of 200.0 MPa.

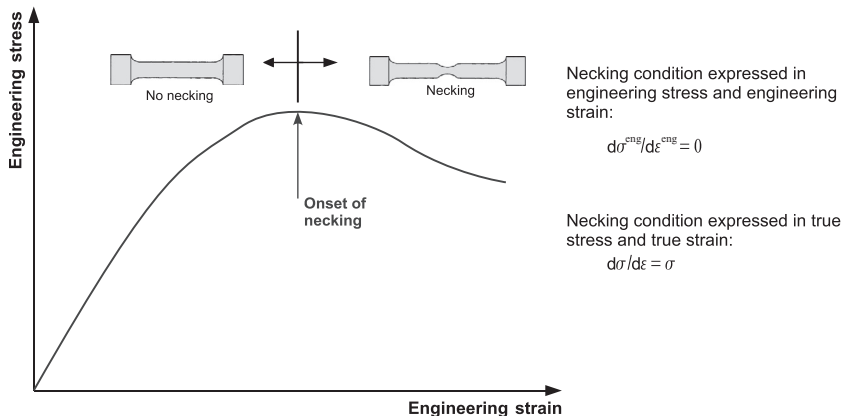


Figure 2.12 Necking of test specimens in uniaxial tension.

however, a small drop in the engineering stress may not lead to a visible neck in tension specimen.

Figure 2.13 shows the progression of the necking from a virtual experiment. In this case, a material model with strong stress softening after yielding was selected using the Parallel Network Model from the PolyUMod library (see Section 8.7). The ASTM D638 Type IV specimen was then simulated with that material model. As shown in the figure, the necking starts relatively early and a stable neck is then propagated along the gauge section of the specimen until it has reached a maximum length. At that time the total force starts to increase again.

Note that only some polymer neck when loaded in tension. For example, elastomers do not neck, LDPE and HDPE undergo necking, but UHMWPE does not neck.

If the purpose of the experimental testing is to obtain suitable experimental data for material model calibration, then it is still possible to use tension data with necking as long as experimental setup is simulated as part of the calibration procedure. This topic is discussed in more detail in Chapter 9.

2.2.3 Plane Strain Tension

One relatively common loading mode for elastomers is *plane strain tension*. In this test, a wide sheet of material is pulled in

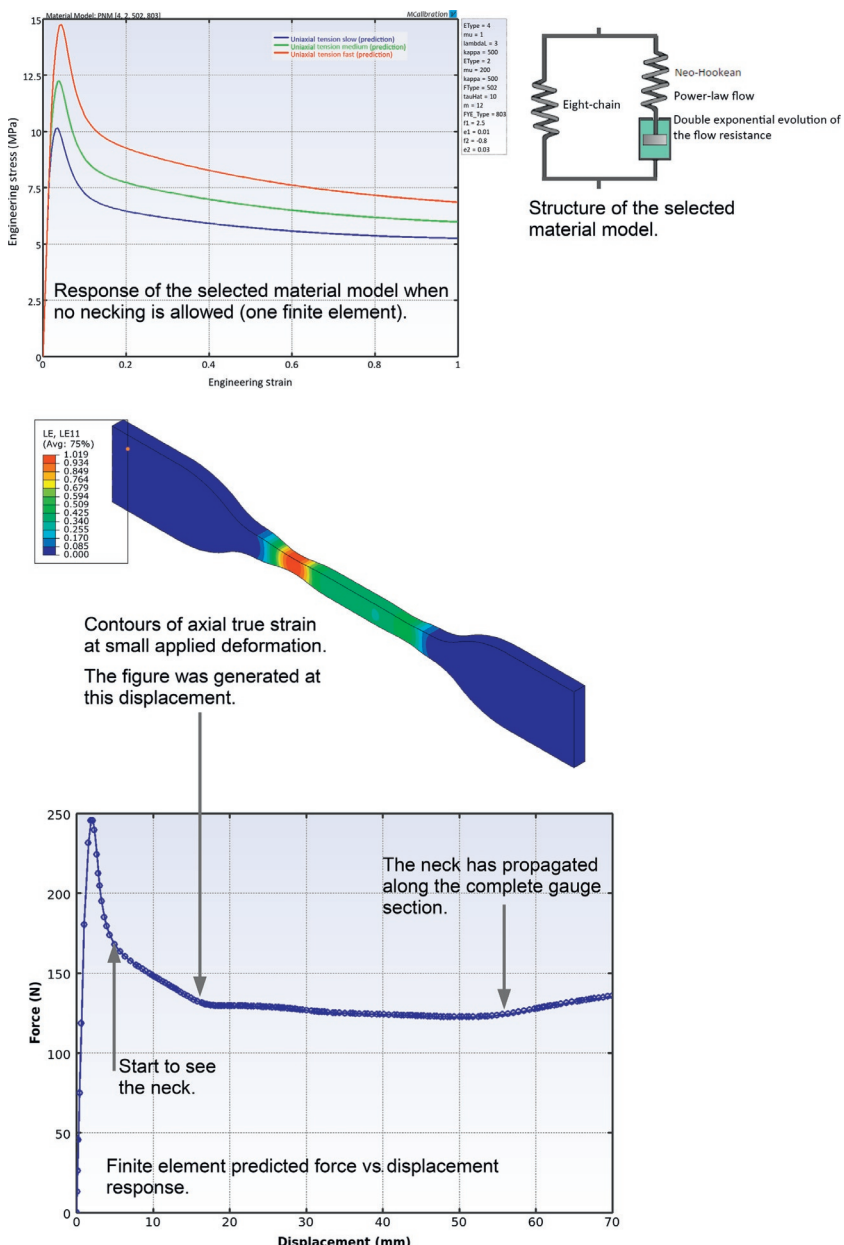


Figure 2.13 Necking of an ASTM D638 IV test specimen pulled in uniaxial tension. The material was modeled using the specified Parallel Network Model.

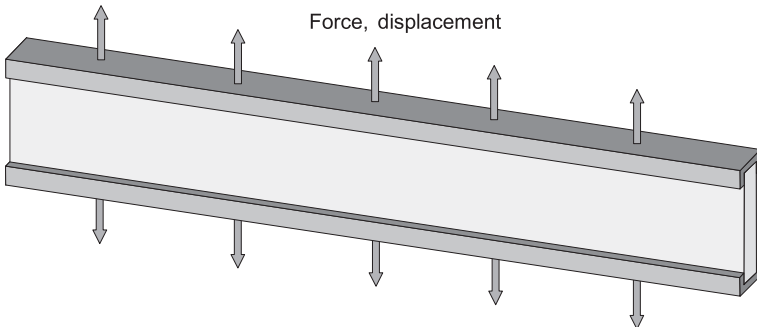


Figure 2.14 Schematic figure showing a plane strain tension specimen.

tension, see [Figure 2.14](#). The general guideline is for the specimen width to be at least 10 times wider than its height. By having a wide specimen, the in-plane displacements will be mainly along the loading direction (and through the specimen thickness). This will ensure that the deformation state is close to plane strain.

In plane strain loading, since there is no contraction of the specimen in its width direction, the thickness strain will be similar in magnitude to the applied axial strain (as long as the material is almost incompressible). As an example, if the applied axial (true) strain is 50% then the strain through the thickness will be approximately -50% . Even if the specimen is gripped with platens that apply a constant pressure, the specimen will thin down at the interface line with the platen edge causing an effective specimen length that increases with the applied strain. Due to this effect it is important to measure the effective axial strain in the center of the specimen. This can be achieved by using a laser extensometer or a digital image correlation strain measurement system.

The influence of the specimen width on how close the deformation state is to the desired plane strain deformation state is examined in [Figures 2.15](#) and [2.16](#). These figures show the results from an FE study that is using one-eighth symmetry, and a Neo-Hookean material model with a shear modulus of 2 MPa and a bulk modulus of 200 MPa. In the simulation, the specimen was gripped using an analytical rigid surface that was pushed against

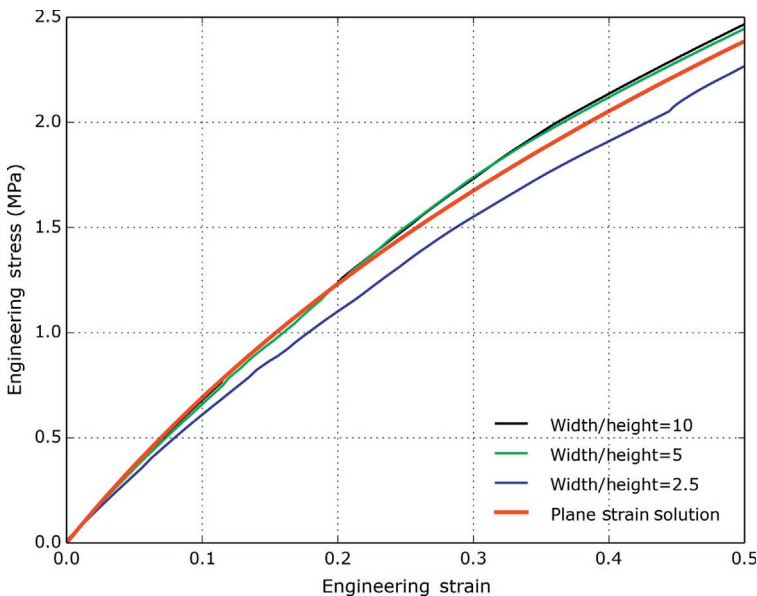


Figure 2.15 Influence of specimen width on the stress-strain response.

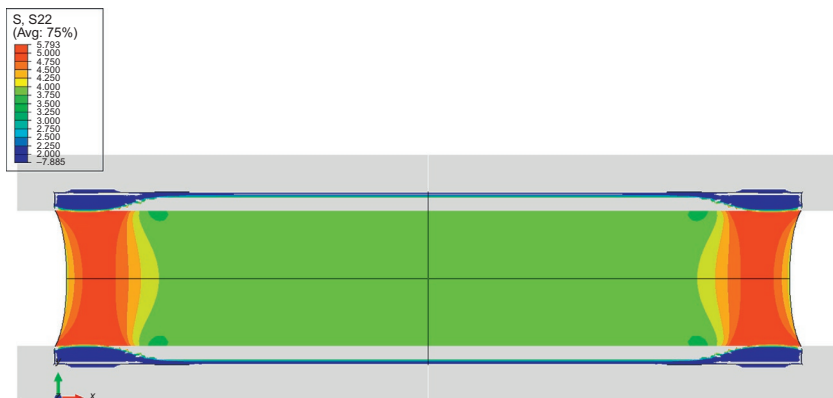


Figure 2.16 Contours of vertical stress in a plane strain test specimen that is 10 times wider than its initial height. The applied engineering strain (at the crosshead) is 0.8.

the specimen with a force per grip length of 10 N/mm. The friction coefficient between the specimen and the simulated loading platen was 1.0.

The thick red line in this figure shows the true plane strain response, the blue line shows the response if the specimen is 2.5 times wider than its initial height, the green and the black lines show the response for 5 and 10 times wider than the initial height. The FE results show that having a specimen width of only 2.5 times the initial height is not sufficient for introducing a mainly plane stress-strain state, and that if the width is 5 or 10 times the initial gauge section length then the determined stress will have an error that is less than 9% at an applied effective strain of 50%.

One other experimental complication of the plane strain tension test is that it is often necessary to grip the specimen relatively tight in order to avoid specimen slippage at the grips. This can cause a stress concentration close to the grips, and since the specimen is not dog-bone shaped, may influence the stress and strain state inside the specimen.

2.2.4 Simple Shear Testing

As will be discussed in Chapter 5, most finite strain material models for polymers divide the mechanical response into distinct shear and volumetric behaviors. Based on this decomposition of the deformation it is sometimes desirable to directly measure the shear response of a material. This can be achieved, for example, by performing torsion experiments. But since torsional test machines are still relatively uncommon, it is valuable to be able to determine the shear response using a more common uniaxial loading machine. A frequently used technique to measure the shear response is to use a single-lap or double-lap shear setup, as shown in [Figure 2.17](#).

The results from single- and double-lap shear experiments can be quite different. The single-lap shear test is not self-centering and the top and bottom regions need to be tightly gripped in order to avoid specimen rotation which will result in a deformation

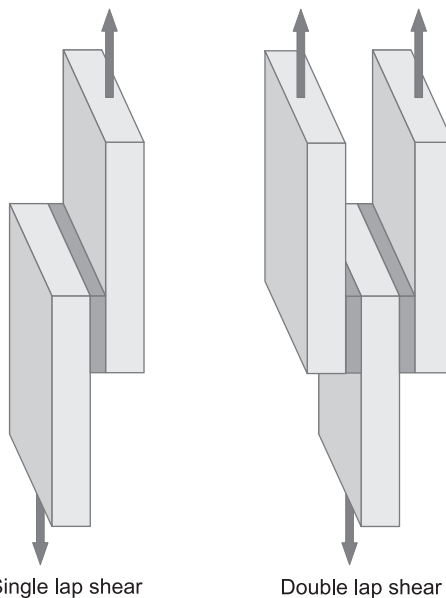


Figure 2.17 Schematic figures of single-lap and double-lap shear specimens. The dark blue regions are the test specimens.

state that is not consistent with simple shear. The symmetry of the double-lap shear test removes most issues related to specimen rotations, and because of that it is usually easier to both grip and run a double-lap shear test.

To get a deformation state that is mostly simple shear, and that is defined by the deformation gradient

$$\mathbf{F} = \begin{bmatrix} 1 & \gamma & 0 \\ 0 & 1 & 0 \\ 0 & 0 & 1 \end{bmatrix}, \quad (2.2)$$

where γ is the applied displacement divided by the specimen thickness, it is important that the thickness of the specimen is small relative to the two other in-plane dimensions.

Figure 2.18 shows the results from an FE study aimed at examining the error that can be expected in a simple lap or double lap shear experiment. In this case, the specimen is assumed to have a base area of $10\text{ mm} \times 10\text{ mm}$, and different

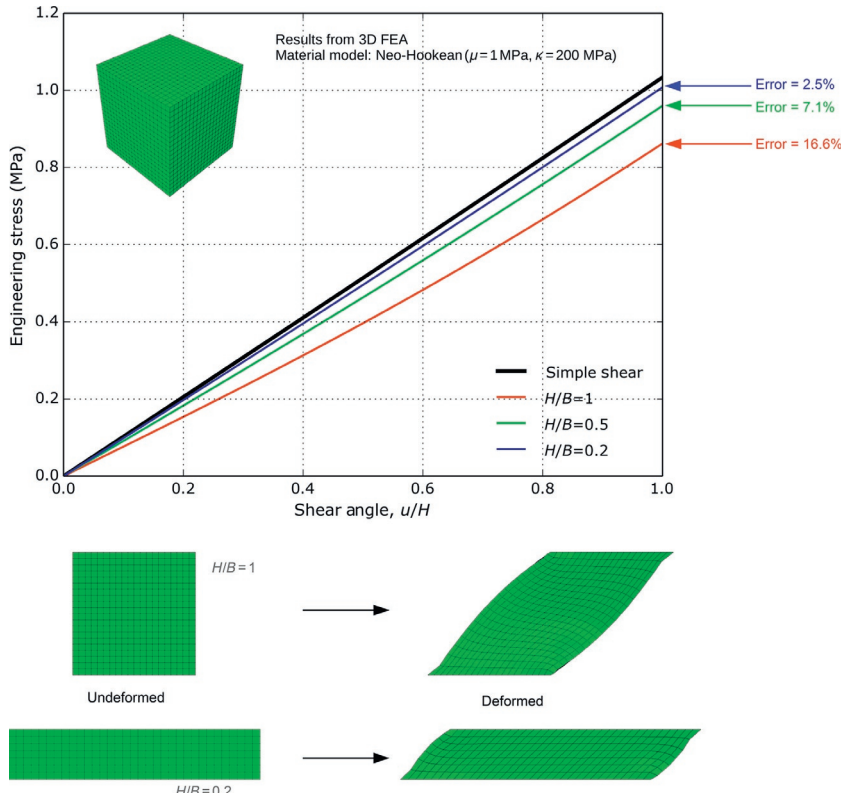


Figure 2.18 FE results showing the influence of specimen dimensions on the simple shear stress. Neo-Hookean material model with a shear modulus of 2 MPa and a bulk modulus of 200 MPa.

specimen heights (thicknesses) were examined. The material was represented using a Neo-Hookean hyperelastic model with a shear modulus of 2 MPa and a bulk modulus of 200 MPa. The specimen was assumed to not rotate during the loading, and the specimen was assumed to be perfectly bonded to the loading platens.

The results from the study show that the accuracy is increased (and the loading mode more similar to simple shear) for specimens with a small height to base width. As an example, if the specimen width (and depth) is five times larger than the specimen height, then the error in the predicted shear stress is about 2.5%.

2.2.5 Impact Testing

In the traditional experimental stress-strain tests, discussed in Sections 2.2.1–2.2.4, the test specimens are typically loaded at a quasi-static rate. In many real applications, however, polymer components are often exposed to rapid impact loads: for example, impact after free falling, or direct blows or collisions. The purpose of performing mechanical impact tests is to simulate these conditions more directly and to examine the mechanical behavior of polymers under impact conditions.

Two commonly used impact testing methods for polymers are the *Izod* and *Charpy* tests. Both the Izod and the Sharpy tests are performed using a pendulum impact machine, see Figures 2.19 and 2.20.



Figure 2.19 Typical analog (noninstrumented) impact testing machine. (Reproduced with permission from Qualitest, www.WorldofTest.com.)

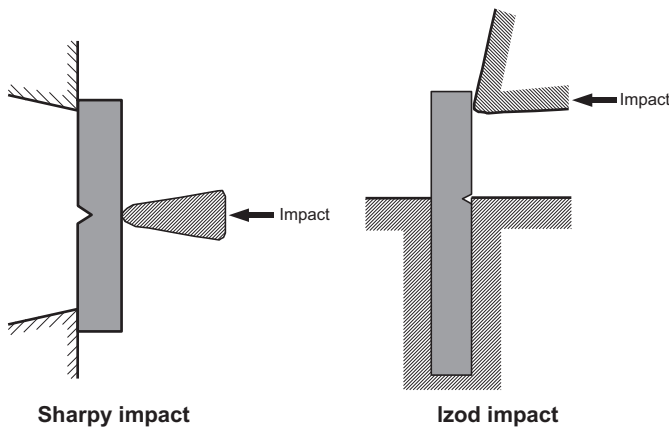
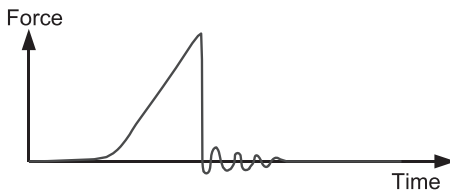


Figure 2.20 Test specimen geometry used in Sharpy and Izod impact testing.

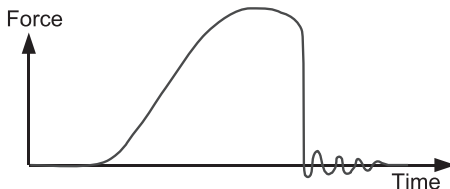
In the tests, the specimen is positioned in a vice, and the pendulum hammer is released from a predefined height. The residual kinetic energy in the hammer after the specimen has been broken carries the hammer upward to a final location. The energy required to break the specimen can be directly obtained from the initial drop height and the final drop height. The impact tests are routinely performed over a wide temperature interval to examine ductile-brittle transitions. The tests are also often performed with different specimen geometries, and with specimens with or without notches.

There are two basic ways in which the impact tests can be performed: noninstrumented or instrumented. A noninstrumented impact test only measures the energy required to break the specimen, whereas an instrumented impact test also measures the force history during the impact, see [Figure 2.21](#). In the instrumented impact tests, the pendulum's hammer is equipped with a load cell, and the impact data are stored using a high-speed data acquisition system enabling extraction of not only the energy required to cause failure but also force and velocity as a function of time. This measured force can be used to distinguish between brittle and ductile fracture, and can be used to extract information about the required energies for crack initiation and

Brittle failure:
• Fully brittle failure



Brittle/ductile failure:
• Some yielding before rapid brittle failure



Ductile failure:
• Fully ductile failure

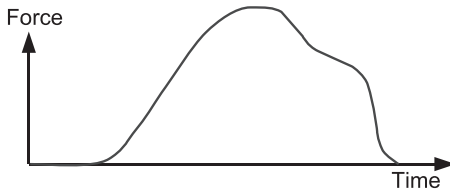


Figure 2.21 Schematic test results from an instrumented Izod or Sharpy impact test.

crack propagation. Note that the most commonly used impact-test standards do not call for instrumentation [7, 8].

Due to the complicated evolution in multiaxial stress and strain during the impact event, the results from these impact tests are typically not useful for determining true material properties or for calibrating constitutive models. What the tests are useful for is to provide relative ranking of impact strength between different materials. As a further complication, the impact properties can be very sensitive to test specimen thickness and molecular orientation. The differences in specimen thickness as used in the ASTM and the ISO standard methods may affect impact properties strongly [7–10].

Both the Izod and the Sharpy impact tests can present experimental challenges. One of the main weaknesses of the Izod impact test is that it tends to measure notch sensitivity instead of inherent impact toughness. To overcome this weakness is sometimes unnotched Izod tests performed. Another weakness of the Izod test is that the force used to clamp the sample can vary between

tests, and the force creates an initial stress state in the specimen. These complications often increase the statistical variations in the impact test results. A final weakness of both Izod and Sharpy tests is that incorrect or inconsistent notching of test specimens can cause significant variability.

The in-plane tensile impact resistance of polymer films is tested using a different experimental approach. These impact tests are typically performed using the Gardner falling weight method for rigid materials [11] or dart drop for films [12]. In these tests, a weight is placed at the end of a nub or dart that is raised to a specific height and dropped on the secured specimen. The drop tests are typically incremental, requiring a relatively large number of test specimens to determine the failure energy. The energy absorbed during the impact is calculated based on the contact area, weight, and drop height of the impact object. Due to the strain-rate dependence of polymers, a 2 kg weight dropped from 1 m impart the same amount of energy as a 20 kg weight dropped from 0.1 m, but the two cases can result in different behaviors due to different impact velocities. These tests typically provide pass/fail data: they give the average impact energy that breaks the sample 50% of the time. If the falling dart is instrumented then these tests can also be used for material model calibration by using FE simulations of the experimental setup.

The high strain-rate response of many materials that are only available in challenging specimen geometries can also be evaluated using impact tests. As an example, instrumented ball impact testing can very accurately determine the through thickness response of thin films and pressure sensitive adhesives [13].

2.2.6 Dynamic Mechanical Analysis

Dynamic mechanical analysis (DMA) is a useful technique for experimental characterization of the small-strain viscoelastic properties of polymers [14–17]. DMA measures the stiffness and viscoelastic damping properties under dynamic vibrational loading at different temperatures. The technique is applicable to virtually all polymers, including elastomers, thermoplastics,

thermosets, and films and fibers of these materials. DMA is an interesting technique because of its ease of use and its ability to extract large amounts of experimental data from a few experimental tests. It is also one of the most sensitive analysis techniques for determining, for example, the glass transition temperature T_g .

In DMA experiments, a specialized testing machine applies a sinusoidal force or displacement to a test specimen and the resulting response is measured. For viscoelastic materials the measured response lags behind the input stress wave with respect to its phase angle and this lag is known as the phase angle, δ . As is discussed in more detail in Chapter 6, an effective modulus, called the complex modulus, E^* can be obtained by dividing the stress amplitude with the strain amplitude. The complex modulus can be further decomposed into a storage modulus E' , which is in-phase with the applied loading, and a loss modulus E'' , which is out of phase with the applied loading. The storage modulus is directly related to the energy storage capabilities of the material, and the loss modulus is related to the dissipated heat (hysteresis). Another commonly used quantity is $\tan(\delta)$, which is the ratio of the loss modulus to the storage modulus, that is $\tan(\delta) = E''/E'$. The quantities E' , E'' , and $\tan(\delta)$ are strong functions of temperature and loading frequency. The goal of DMA experiments is to determine how these viscoelastic quantities depend on temperature and loading frequency.

The experimental procedure to perform DMA is described both in ASTM [16] and ISO standards [17]. The DMA experiments can be performed in many different loading modes, for example, uniaxial tension, compression, shear, bending, or torsion. The experimental setup is driving the deformation either at resonance frequency or using forced vibration. Which loading mode and approach that is used in the experiment is determined by the particular DMA test machine that is used. For solid polymers the most common experimental approach is to select a constant frequency and amplitude of the vibration, and then measure the material response as a function of temperature. Following standard guidelines [16, 17], the temperature is swept either in a stepwise manner with constant temperature increments that are held for a

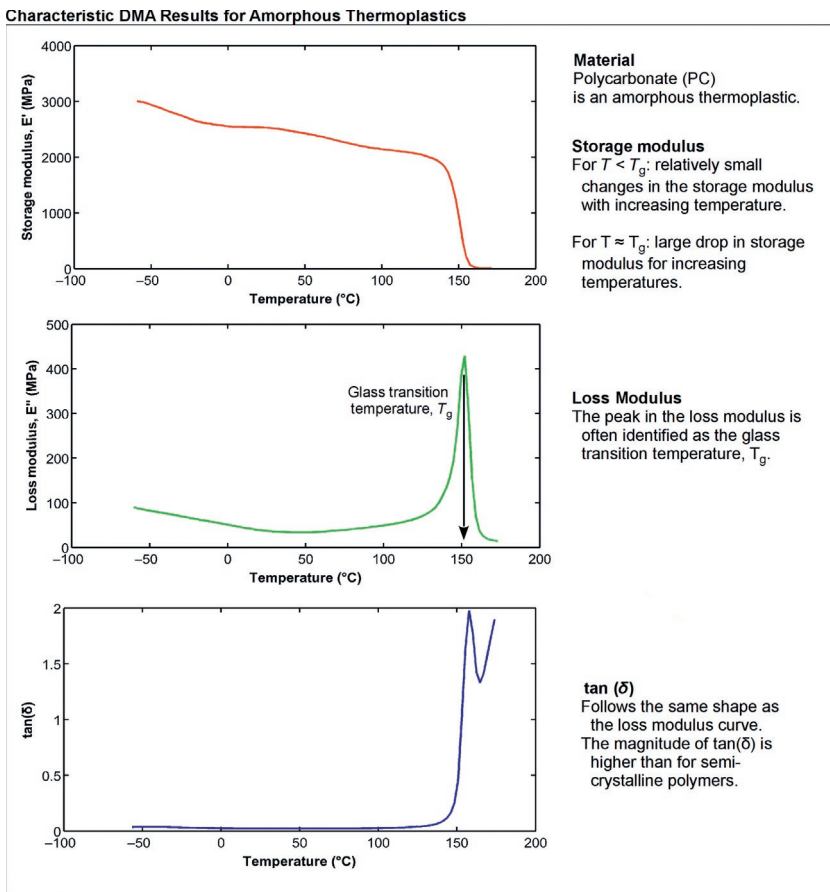


Figure 2.22 Exemplar DMA test results for polycarbonate which is an amorphous thermoplastic polymer.

certain time before the dynamic measurements are made, or by applying a constant heating rate, often about $2\text{ }^{\circ}\text{C}/\text{min}$.

Exemplar DMA result for amorphous and semi-crystalline thermoplastics are shown in Figures 2.22 and 2.23. Figure 2.22 shows the storage modulus (E'), loss modulus (E''), and $\tan(\delta)$ for polycarbonate, an amorphous thermoplastic. The figure shows that both the storage modulus and the loss modulus are only weakly dependent on temperature for temperatures $T < T_g - 30\text{ }^{\circ}\text{C}$. In the temperature range from $T_g - 30\text{ }^{\circ}\text{C}$ to $T_g + 30\text{ }^{\circ}\text{C}$, the storage modulus goes from an initially high value down to

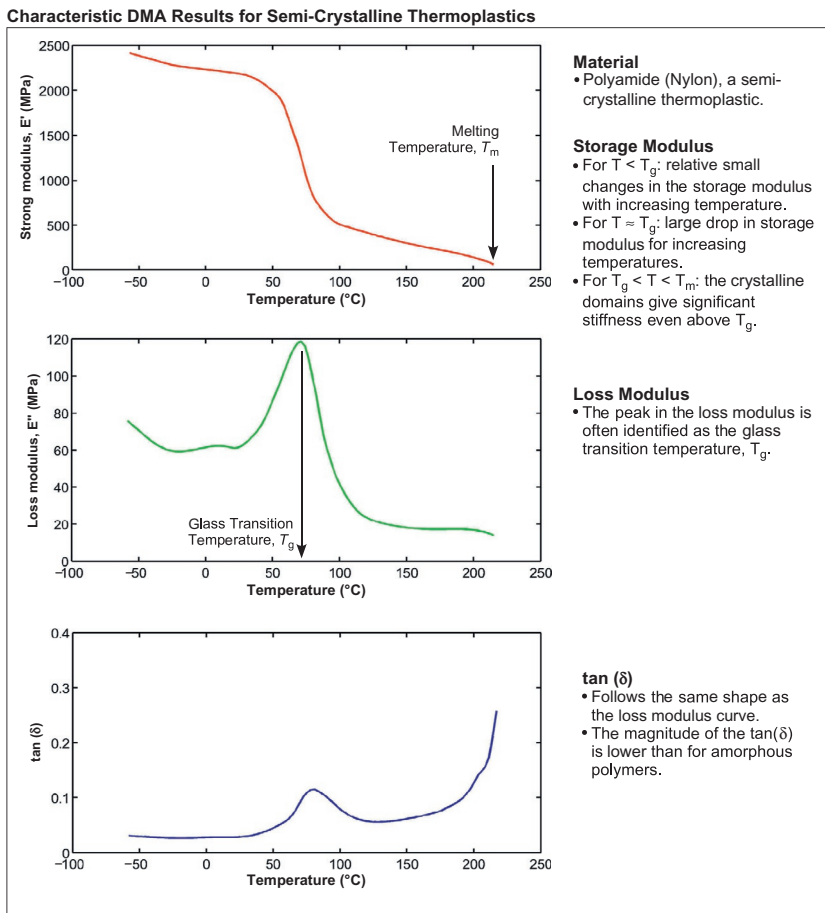


Figure 2.23 Exemplar DMA test results for nylon which is a semi-crystalline thermoplastic polymer.

virtually zero stiffness. In the same temperature interval, the loss modulus exhibits a peak due to the enhanced mobility of the amorphous microstructure from thermal energy. The temperature at which the loss modulus reaches its peak value is often taken as the glass transition temperature, T_g . Since $\tan(\delta)$ value is given by E''/E' , the overall shape of $\tan(\delta)$ is similar to the shape of E'' .

Figure 2.23 shows the DMA data for polyamide (Nylon), a semi-crystalline thermoplastic. The storage modulus is at low

temperatures only weakly dependent on the temperature, but undergoes a drastic reduction around T_g . Due to the crystalline domains of the microstructure, the storage modulus stays finite at temperatures that are above T_g but below the melting temperature of the crystalline domains. For this reason, semi-crystalline polymers can often be used as structural components even at as high temperatures as $T_g + 100\text{ }^\circ\text{C}$. The loss modulus and the $\tan(\delta)$ function follow a similar trend as for amorphous thermoplastics. Due to the integrity of the crystalline domains, $\tan(\delta)$ is typically much smaller for semi-crystalline thermoplastics compared with amorphous thermoplastics.

2.2.7 Hardness and Indentation Testing

The hardness of a polymer is an empirical quantity related to the inherent indentation resistance. The two most common methods for measuring polymer hardness are the Rockwell hardness test [18] and the Shore (durometer) hardness test [19].

These tests provide a fast and easy method to characterize the hardness of a polymer. They are useful for ranking the hardness of different polymers, but do not necessarily provide results that correlate with other fundamental material properties.

Rockwell Hardness Testing

The Rockwell hardness test is typically chosen for stiff thermoplastics, such as polycarbonate and polystyrene. For these materials the resistance to viscoelastic flow below the glass transition temperature is almost time-independent and the extracted hardness values are therefore also almost time-independent.

Rockwell hardness tests are typically performed following ASTM D785 [18]. In this test specification, a specimen with a thickness of at least 6 mm is indented by a steel ball. A small load is applied on the indenter, the indentation displacement is recorded, and then a larger load is applied and removed. After a

short time, with the preload still applied, the remaining indentation is determined and used to calculate the hardness value.

Different Rockwell hardness scales utilize different-size steel balls (between 3 mm and 13 mm) and different loads (between 60 kg and 150 kg). The three most common scales used for plastics are Rockwell E, Rockwell M, and Rockwell R. The correlation between the Rockwell scales is weak; attempts at conversion between the scales are therefore discouraged.

The results obtained from this test provide a useful measure of relative resistance to indentation of various types of plastics. However, the Rockwell hardness test does not serve well as a predictor of other properties such as strength or resistance to scratches, abrasion, or wear, and should not be used alone for product design specifications.

Shore (Durometer) Testing

The Shore (Durometer) test is the preferred hardness testing method for elastomers and is also commonly used for compliant plastics such as polyolefins, fluoropolymers, and vinyl polymers. Shore hardness testing is typically performed following ASTM [19] standards. The two most common test procedures are the Shore A and the Shore D scales. The Shore A scale is used for “softer” rubbers while the Shore D scale is used for “harder” ones. Other Shore scales, such as Shore O and Shore H hardness, are used less often.

The Shore hardness is measured with an apparatus known as a Durometer (see [Figure 2.24](#)) and the determined hardness values are therefore referred to as *Durometer hardness*. The hardness value is determined by the indentation distance into the sample. The type of indenter and applied load is determined by the durometer hardness scale. Due to the viscoelastic behavior of rubbers and plastics, the indentation reading may change over time—so the indentation time is sometimes reported along with the hardness number.

The results obtained from these tests provide a useful measure of relative resistance to indentation of various grades of polymers.



Figure 2.24 Photograph of an exemplar analog durometer.
(Reproduced with permission from Veryst Engineering,
www.veryst.com.)

As for the Rockwell hardness, the Shore Durometer hardness value does not provide direct information of other properties such as strength or resistance to scratches, abrasion, or wear, and should not be used alone for product design specifications.

The correlation between the different Shore Durometer hardness scales is weak, and attempts at converting between the scales are discouraged. Similarly, conversion between Shore hardness and Rockwell hardness is discouraged. Despite these limitations it can be useful to show a rough indication of how the different hardness scale are correlated. [Figure 2.25](#) shows a schematic of the different hardness scales.

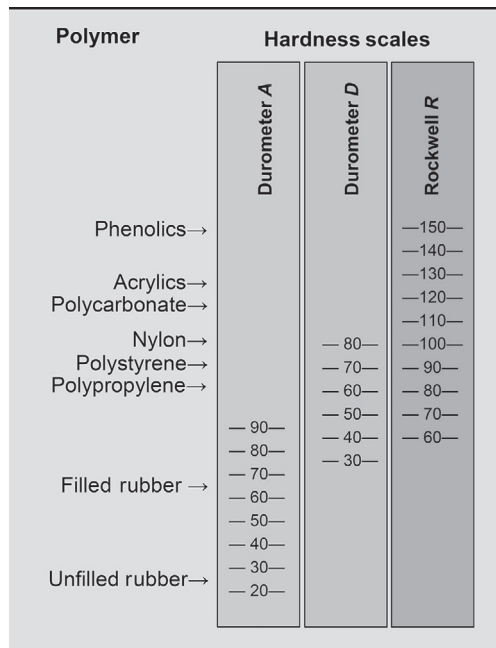


Figure 2.25 Hardness scales used for different classes of polymers. Durometer A and D are primarily used for elastomers and soft thermoplastics. The Rockwell hardness test is often used for stiff thermoplastics.

Barcol Hardness Testing

Barcol hardness is a third hardness test that is used to determine the hardness of both reinforced and nonreinforced thermoset polymers using a barcol impressor. The test procedure is described in ASTM D2583 [20]. The test procedure is portable and therefore suitable for both field testing and quality control testing. The indenter is a truncated steel cone that is loaded onto the test specimen.

As for the other hardness tests, the barcol hardness test does not provide direct information of other mechanical properties, and should only be used as a relative ranking of hardness.

Nanoindentation

Instrumented microindentation and nanoindentation can be quite useful for evaluating the nonlinear viscoplastic response of many different polymers. It is particularly suitable for cases where it would be difficult to extract large enough or otherwise suitable test specimens for the more traditional testing techniques.

Typically a nanoindentation test system is operated by applying a known force on the indenter rod, which is then loading the test specimens through a specified indenter tip. The applied displacement is determined from an accurate capacitance gauge, see [Figure 2.26](#).

One example of the results that can be obtained from a nanoindentation test is shown in [Figure 2.27](#). In this case, a hydrogel material was tested using a nanoindenter run in load-control mode. The specimen was loaded using multiple load-unload segments with inserted creep segments. The results from this test illustrate that the hydrogel undergoes significant creep under the tested conditions. A suitable material model can be calibrated to this data set by inverse calibration using FE simulations of the specific loading geometry and history.

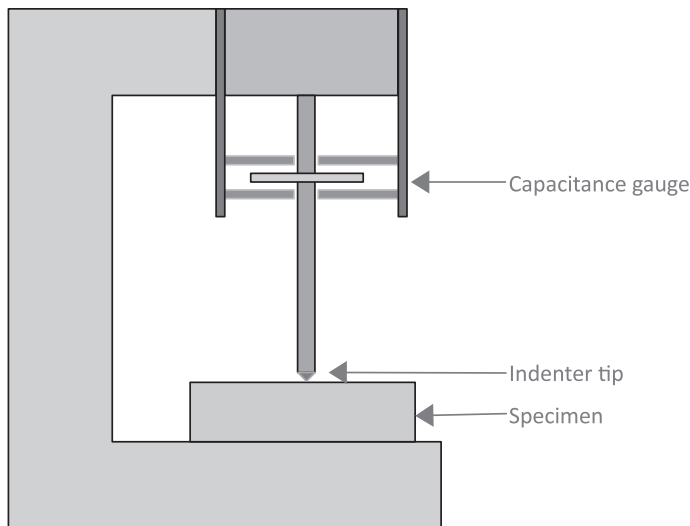


Figure 2.26 Schematic of a nanoindentation setup.

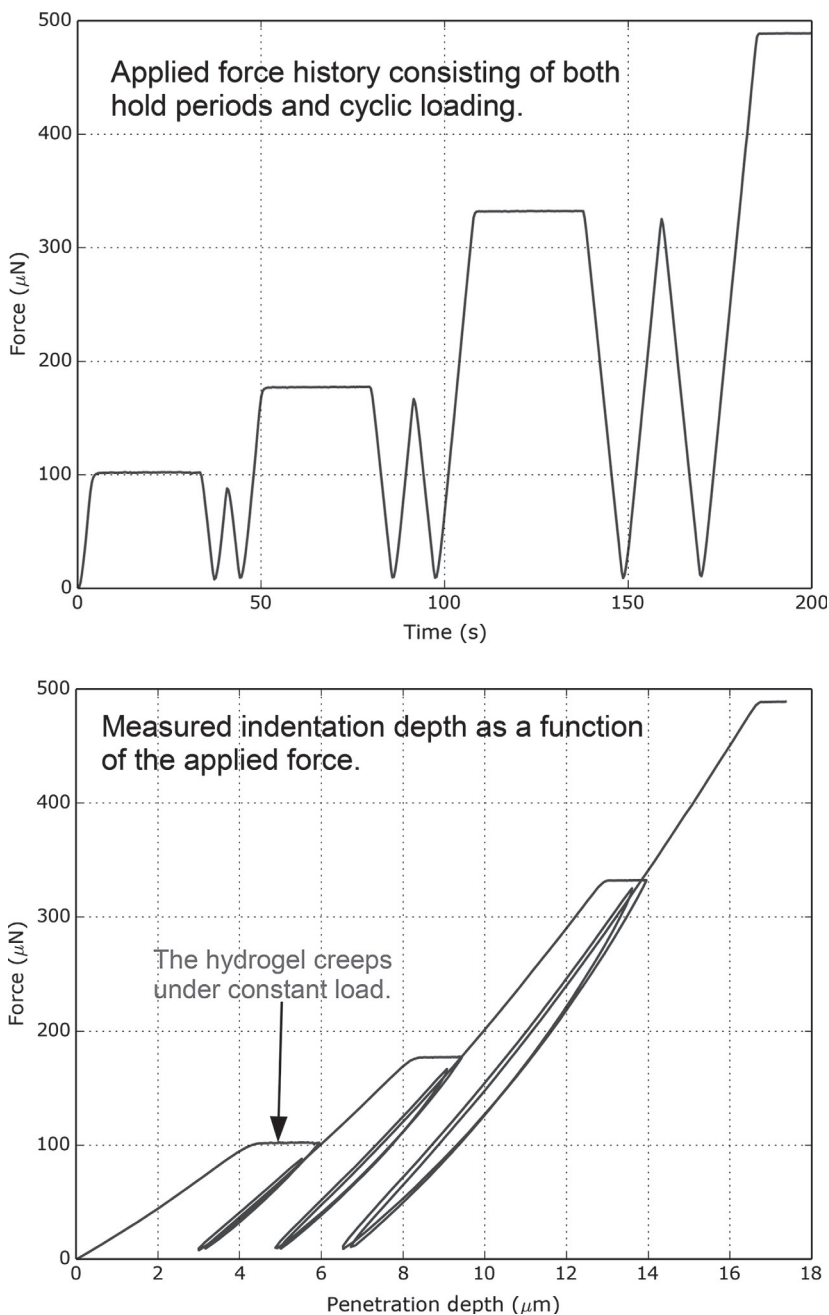


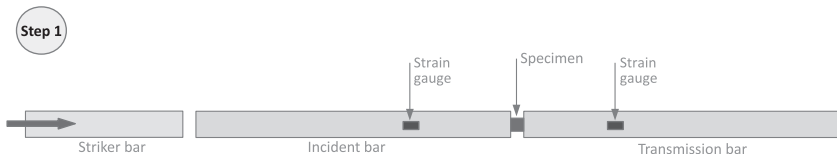
Figure 2.27 Exemplar nanoindentation testing of a hydrogel material. The material exhibits a nonlinear viscoelastic response.

2.2.8 Split-Hopkinson Pressure Bar Testing

Measuring the high strain-rate response of polymers can be very important for many industrial applications where a component is rapidly loaded, for example in drop tests or impact situations. The mechanical response of different adhesives, elastomers, and thermoplastics can be strongly dependent on the loading rate. For this reason, it is important to be able to quantify the material response also at very high strain rates. The most common way to achieve this is to use a *Split-Hopkinson Pressure Bar* (SHPB) test system, which is also called a *Kolsky bar*. The SHPB approach can be applied in different loading modes, including tension, compression, torsion, etc. This section focuses on an SHPB system operating in a compressive mode, additional information for other loading modes is given in the book by Chen and Song [21].

A traditional compressive SHPB system consists of a striker bar, an incident bar, a test specimen, and a transmission bar (see [Figure 2.28](#)). The striker bar, the incident bar, and the transmission bar are typically made from aluminum or steel, but sometimes a polymer (e.g., poly(methyl methacrylate) or polycarbonate) is also used. At the start of an SHPB test, all components are stationary and the specimen is positioned between the incident bar and the transmission bar. Then the striker bar is launched horizontally from a gas gun. The striker bar hits the incident bar and as a result creates an elastic compressive stress wave that travels down the incident bar. Since the incident bar and the transmission bars are designed to be long and slender the stress waves will be essentially one-dimensional. The time history of the stress wave in the incident bar is measured using a strain gauge located a known distance from the specimen. Once the stress wave in the incident bar reaches the specimen interface, part of the wave propagates into the specimen and part of the wave is reflected as a tensile stress wave back in the incident bar. The strength of the reflective wave is then measured again using the same incident bar strain gauge.

The part of the stress wave that goes through the test specimen will create a compressive deformation field inside the specimen.



Initially the incident bar, the specimen, and the transmission bar are all stationary. The striker bar is then launched horizontally with a gas gun.

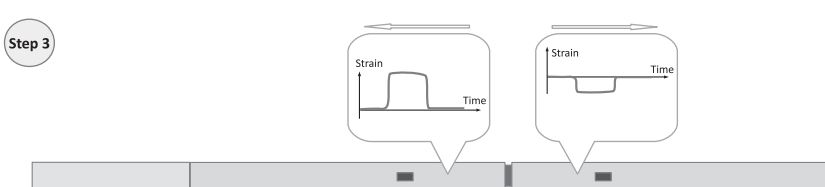


Figure 2.28 Schematic picture of a compressive SHPB system.

That stress wave will then propagate through the transmission bar. The strength of the transmitted stress wave is measured by a second strain gauge located at a known location along the transmission bar.

A schematic picture of an SHPB system is shown in [Figure 2.28](#), and a photograph of an exemplar system is shown in [Figure 2.29](#).

The elastic wave speed in the bars is given by: $C_b = \sqrt{E_b/\rho_b}$, where E_b is the Young's modulus of the bar and ρ_b is the density of the bar. As an example, if aluminum bars are used, then the Young's modulus is given by: $E_b = 72.4$ MPa, the density is $\rho_b = 2700$ kg/m³, giving a wave speed of $C_b = 5178$ m/s. So



Figure 2.29 Photograph of an SHPB system. (Reproduced with permission from Veryst Engineering, www.veryst.com.)

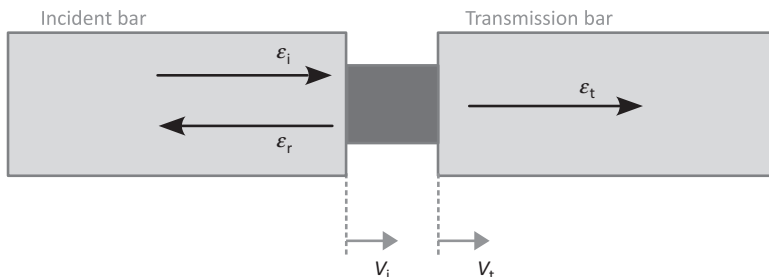


Figure 2.30 Definition of incident, transmitted, and reflected strains at the specimen interfaces in an SHPB test.

if the incident bar is $L_s = 2$ m long, then it will take $t = L_s/C_b = 0.4$ ms for the wave to reach the specimen.

The stress and strain in the test specimen can be calculated from the signals from the incident bar strain gauge and the transmitted bar strain gauge, see Figure 2.30.

The effective engineering strain rate in the specimen is given by:

$$\dot{\varepsilon}_s = \frac{v_i - v_t}{L_s} = \frac{C_b}{L_s} (\varepsilon_i - \varepsilon_r - \varepsilon_t), \quad (2.3)$$

where v_i is the speed of the incident side of the specimen, v_t is the speed of the transmission bar side of the specimen, and L_s is the specimen length. The engineering stress on the incident side of the specimen is:

$$\sigma_i = \frac{A_b}{A_s} E_b (\varepsilon_i + \varepsilon_r), \quad (2.4)$$

where A_b is the cross-sectional area of the bar and A_s is the cross-sectional area of the specimen. The engineering stress on the transmitted side of the specimen is:

$$\sigma_t = \frac{A_b}{A_s} E_b \varepsilon_t. \quad (2.5)$$

If the specimen is in stress equilibrium then $\sigma_i = \sigma_t$, which gives $\varepsilon_i + \varepsilon_r = \varepsilon_t$. Since the three strains $[\varepsilon_i, \varepsilon_r, \varepsilon_t]$ are measured, the experimental strain values can be used to assess if the specimen was in stress equilibrium during the experiment.

Based on these signals, the engineering stress history in the specimen can be calculated from:

$$\sigma_s(t) = \frac{A_b}{A_s} E_b \varepsilon_t(t). \quad (2.6)$$

The engineering strain rate in the specimen is given by Equation (2.3) together with the stress equilibrium condition:

$$\dot{\varepsilon}_s = -\frac{2C_b}{L_s} \varepsilon_r(t). \quad (2.7)$$

The applied engineering strain history in the specimen can be obtained by integrating the strain rate in Equation (2.7):

$$\varepsilon_s(t) = -\frac{2C_b}{L_s} \int_0^t \varepsilon_r(t) dt. \quad (2.8)$$

The details of how an SHPB experiment works can be demonstrated using an FE-based virtual experiment. In this virtual

experiment, the striker bar has a length of 0.3 m and a diameter of 18 mm, the incident bar has a length of 2.3 m and a diameter of 18 mm, and the transmission bar has a length of 2.3 m and a diameter of 18 mm. All of these bars are made of aluminum. The specimen has a length of 6.4 mm and a diameter of 6.4 mm. The initial striker bar velocity is 12 m/s.

In the virtual experiment, the specimen is represented using the Three Network (TN) model (see Section 8.6) with material parameters suitable for UHMWPE. An FE model of this system was created and the stress and strain values at different locations in the model was extracted. The FE results from the virtual strain gauge locations were then inserted into the equations derived above in order to calculate the stress and strain response, just like what is done for real experimental data.

The value of using an FE-based virtual experiment is that it can be used to probe the response of the test system components at any time, and the extracted stress-strain results can also be directly compared to the known behavior of the simulated material ([Figure 2.31](#)).

[Figure 2.32](#) shows the measured strain from the FE simulation at the incident bar gauge location. The strain at the incident bar strain gauge is initially zero, and stays zero until the stress wave has traveled from the striker bar impact location to the gauge location. At that time there is a large negative stress at the gauge location until the whole stress wave pulse has propagated to the right. The stress wave then reaches the end of the incident bar where some of the stress wave is propagated into the test specimen, and some of the stress wave is reflected as a tension wave back along the incident bar. This reflected tension wave then reaches the incident bar again.

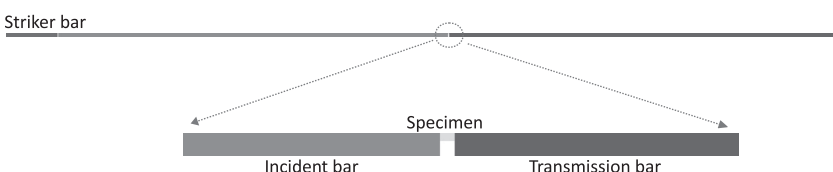


Figure 2.31 Schematic figure of the FE model used in the virtual experiment.

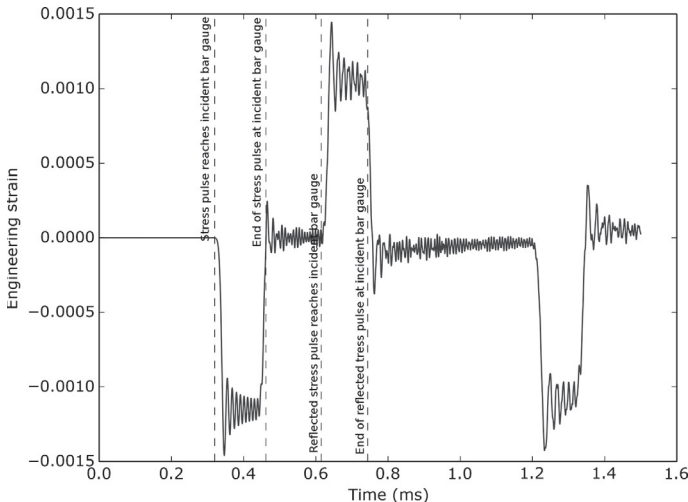


Figure 2.32 Axial strain at the strain gauge location in the incident bar. The strain history is predicted from the FE virtual experiment.

In this example, at a time of 1.2 ms the stress wave in the incident bar has propagated back and forth in the bar and has reached the incident bar strain gauge a second time. As discussed above, this second stress wave is not used in the data analysis.

The FE predicted strain at the transmission bar strain gauge as a function of time is plotted in [Figure 2.33](#). The transmission bar strain remains zero until slightly more than 0.6 s, at which time a compressive stress wave propagates through the strain gauge location. The time when this occurs is very similar to the time at which the reflected stress wave reaches the incident bar strain gauge (as shown in [Figure 2.32](#)).

The wave speed in the polymer specimen is lower than the wave speed in the aluminum bars, but since the specimen length is so small, the time it takes for the stress wave to propagate through the specimen is significantly smaller than the time it takes for the stress wave to propagate from the strain gauge to the end of the bar.

The engineering strain rate in the test specimen (in an average sense) can be calculated from [Equation \(2.7\)](#). This equation shows that the engineering strain rate is directly given by the reflected

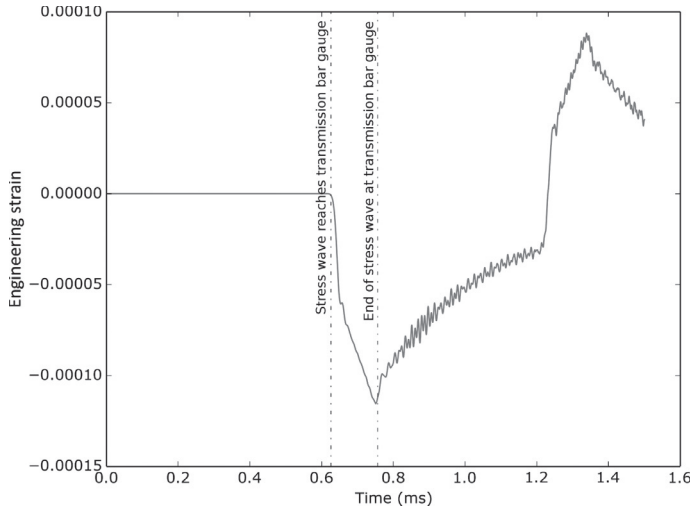


Figure 2.33 Axial strain at the strain gauge location in the transmission bar. The strain history is predicted from the FE virtual experiment.

strain at the incident bar strain gauge, the wave speed in the incident bar, and the test specimen length.

In this case, the engineering strain rate goes very quickly from 0 to about -2000 per second, and then stays at about -1800 per second for the duration of the first stress wave. Note that the strain rate is not constant during the compression of the specimen. This is not a problem since the experimental data from the experiment can be used for material model calibration even if the strain rate is not constant, as long as the time-history of the strain rate is known ([Figure 2.34](#)).

As shown in [Equation \(2.8\)](#), the strain history can be obtained from integrating the strain rate history from the previous figure. This integration can be done quickly using a numerical approach and the results are plotted in [Figure 2.35](#).

The stress in the test specimen can be calculated from [Equation \(2.6\)](#). As shown in this equation, the specimens stress can be obtained from the transmission bar strain gauge data, as shown in [Figure 2.36](#). This figure also shows the strain history of one element in the middle of the test specimen. The stress in this interior element was extracted from the FE postprocessing, and

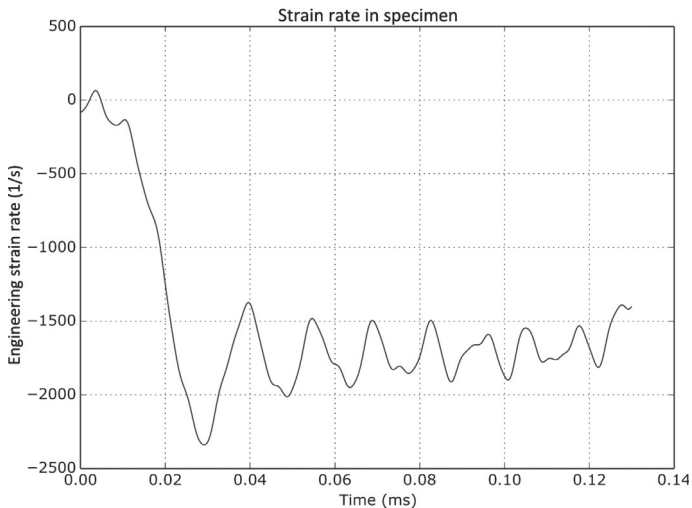


Figure 2.34 Strain rate in the test specimen as a function of time. The strain rate is calculated from the FE virtual experiment data.

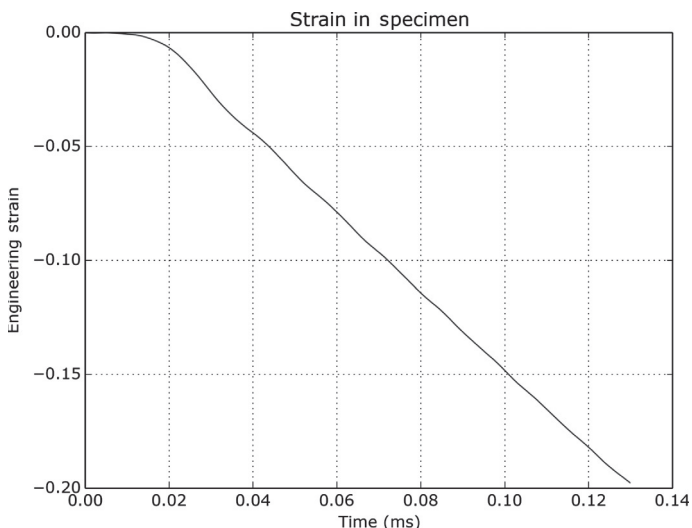


Figure 2.35 Strain history in the test specimen as a function of time. The strain is calculated from the FE virtual experiment data.

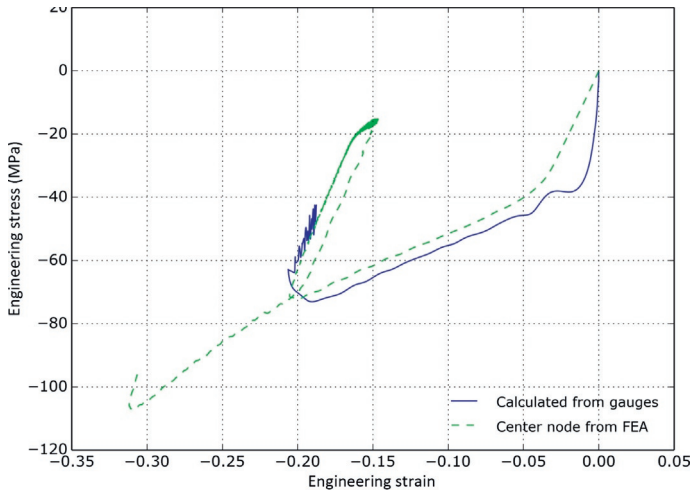


Figure 2.36 Predicted stress in the test specimen in the FE virtual experiment.

since it was not calculated in an approximate way from the strain gauge signals but directly from the selected constitutive model, it represents the true response of the material.

It is interesting to note that the stress-strain response of the interior element undergoes loading, followed by unloading, followed by further loading. This is caused by the displacement field history in the incident bar due to the propagating stress waves. The calculated stress from the strains at the two gauge locations capture the first compression phase and a small amount of the initial unloading. This is typical of SHPB data that is obtained from an experiment on a polymer. The figure also shows that the SHPB technique does not accurately measure the initial stress-strain response at small deformations. The stress-strain response at larger deformations can often be obtained accurately.

The SHPB experiment suffers from the same issue with interface friction as in uniaxial compression. [Figure 2.37](#) shows the stress-strain response when there is no friction and when there is a friction coefficient of 0.4. The only difference between the two curves shown in the figure is the friction coefficient in the interface between the test specimen and the bars.

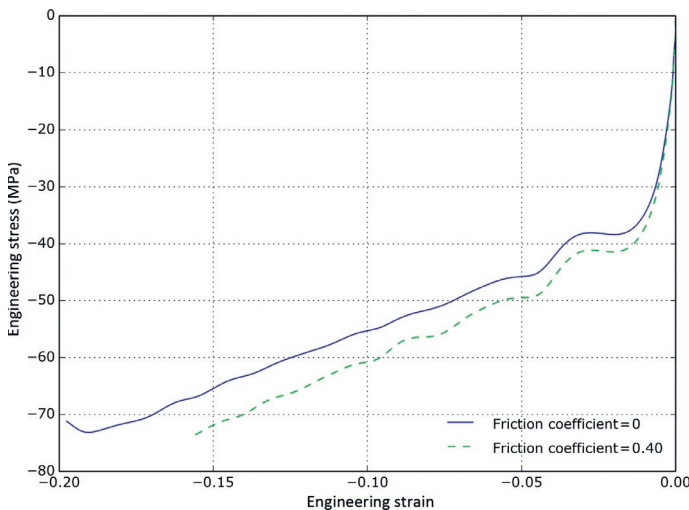


Figure 2.37 Dependence of the predicted stress on the friction coefficient in an FE virtual experiment of an SHPB test.

As expected, the influence of friction is also important for the SHPB test, and the magnitude of how much the stress changes with friction coefficient is similar to what is observed in slow rate uniaxial compression experiments.

One of the limitations of the SHPB test is that it cannot be used to measure the high strain rate response of very soft polymers. If a material is very soft then the wave speed in the material becomes quite low (the wave speed is given by $\sqrt{E/\rho}$) and the specimen will be deformed in an inhomogeneous way during the loading. Also, and equally important, the stress wave that is transmitted from the specimen to the transmission bar strain gauge becomes very low making the calculation of the stress difficult.

One example of this phenomenon is shown in Figure 2.38. The graph in part (a) shows the SHPB prediction, the stress at a center node, and the exact stress-strain response from a TN material model with an initial Young's modulus of 500 MPa.

Figure 2.38(b) shows the same results as in Figure 2.38(a), but for a material with an initial Young's modulus of 100 MPa. This material model was created from the 500 MPa material model by scaling all material parameters with units of stress by a factor of one-fifth. These figures show that the SHPB prediction

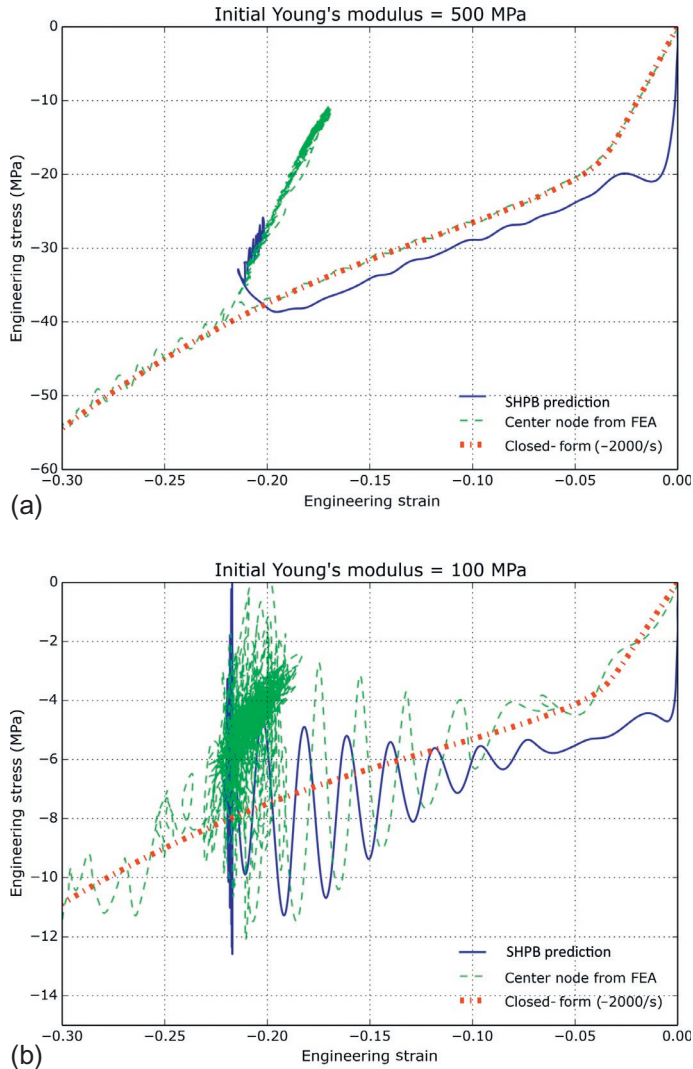


Figure 2.38 Predicted stress in the test specimen in the FE virtual experiment: (a) stress-strain response for a material with an initial Young's modulus of 500 MPa and (b) same results for a material with an initial Young's modulus of 100 MPa.

of the 500 MPa material is accurate and reliable, but that the prediction of the 100 MPa material is not useful. In this case, the 100 MPa material is too soft for accurate characterization using an SHPB test.

2.2.9 Bulk Modulus Testing

It is not necessary to accurately know the bulk modulus (or the Poisson's ratio) of a polymeric material in order to perform accurate FE simulations of most industrial applications. The reason for this is that the bulk modulus has only very limited influence on the mechanical response under most loading modes.

As an example, [Figure 2.39](#) shows the predicted stress-strain response in uniaxial tension for the TN model (see Chapter 8, Section 8.6) with different values for the bulk modulus. In this case, the true stress is reduced by less than 0.5% when the bulk modulus is reduced from 2000 MPa to 500 MPa, corresponding to a change in the small strain Poisson's ratio from 0.47 to 0.40.

In some specific applications, the bulk modulus can influence the component response. One example is an o-ring that is constrained in a groove. [Figure 2.40](#) shows the results from an example in which an o-ring is pressurized in a confined geometry with a small groove. The pressure below the o-ring was 15 MPa. The o-ring material was represented using the BB model

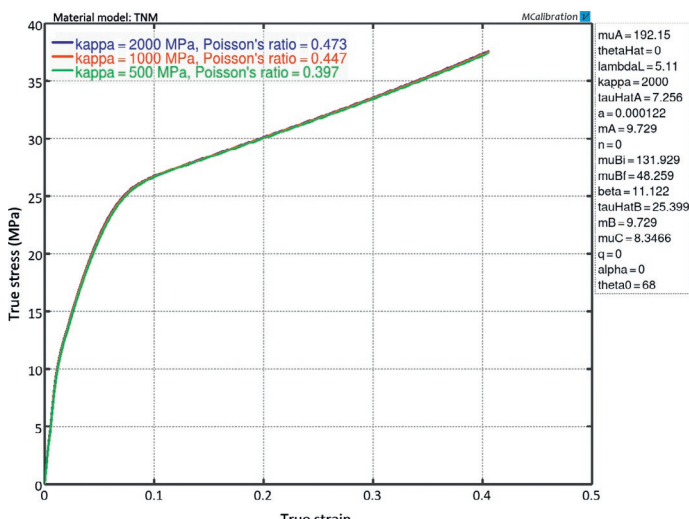


Figure 2.39 Influence of the bulk modulus and initial Poisson's ratio on the predicted stress-strain response in uniaxial tension. The predictions were obtained from the TN model.

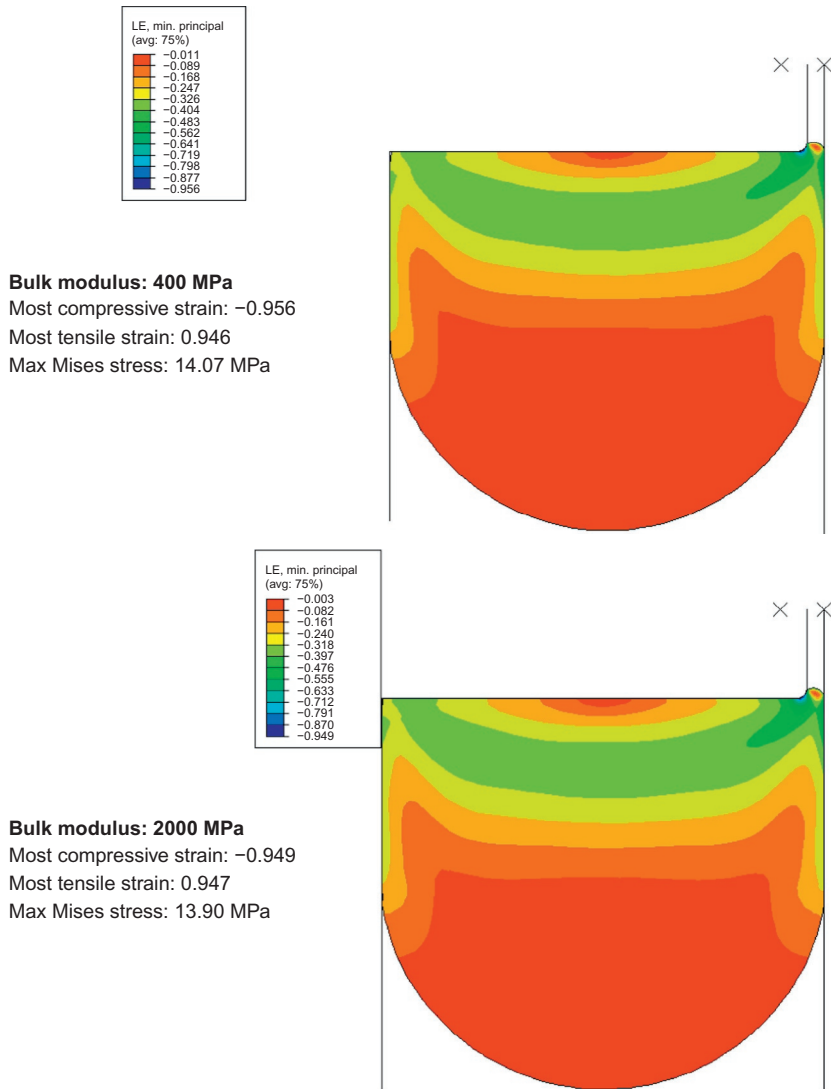


Figure 2.40 Influence of the bulk modulus (and Poisson's ratio) on the predicted response of an o-ring in a confined geometry with a small groove. The predictions were obtained from the BB model.

(see Section 8.2) with material parameters corresponding to a soft rubber. The FE simulation was first run with a bulk modulus of 400 MPa (corresponding to a Poisson's ratio of 0.495), and then with a bulk modulus of 2000 MPa (corresponding to a Poisson's ratio of 0.499).

The results from the FE simulations are shown in [Figure 2.40](#). This figure shows that the o-ring gets severely deformed due to the applied pressure and starts to extrude into the small gap. Note the difference in the predicted max stress and max strain values between the two cases with different bulk moduli is only about 1%.

A second example with a constrained o-ring without a groove is shown in [Figure 2.41](#). This example is exactly the same as the previous example except that there is no gap for the o-ring to extrude into, and the applied pressure was 40 MPa. In this case, the predicted max stress and max strain values between the two cases with different bulk moduli is about 7%.

The bulk modulus of a polymer can be measured using different experimental techniques. One approach is to use a Digital Image Correlation (DIC) strain measurement system that can directly measure both the axial and the transverse strains during a uniaxial tension or compression test. These data can then be used to calculate the Poisson's ratio, and from that the bulk modulus can be calculated using Table 5.1. (see Chapter 5).

Another approach is to use pressure-volume-temperature (PVT) testing [22]. In this technique, the specific volume of a material is measured as a function of the applied pressure and temperature. From that experimental data the bulk modulus can be calculated.

A third method is to use a confined compression test. In this technique, a cylindrical specimen is inserted into a thick-walled cylinder, and then compressed with a cylindrical rod with the same diameter as the diameter of the hole in the thick-walled cylinder. [Figure 2.42](#) shows a schematic of the experimental setup.

In this type of experiment, the force-displacement response of the cylindrical push rod, and the strain on the outside surface of the thick-walled cylinder are measured. From these signals the pressure-volume response of the polymer can be determined, from which the bulk modulus is calculated from the slope of the calculated pressure-volume response. One benefit of this approach is that it can be performed at a wide temperature and pressure range.

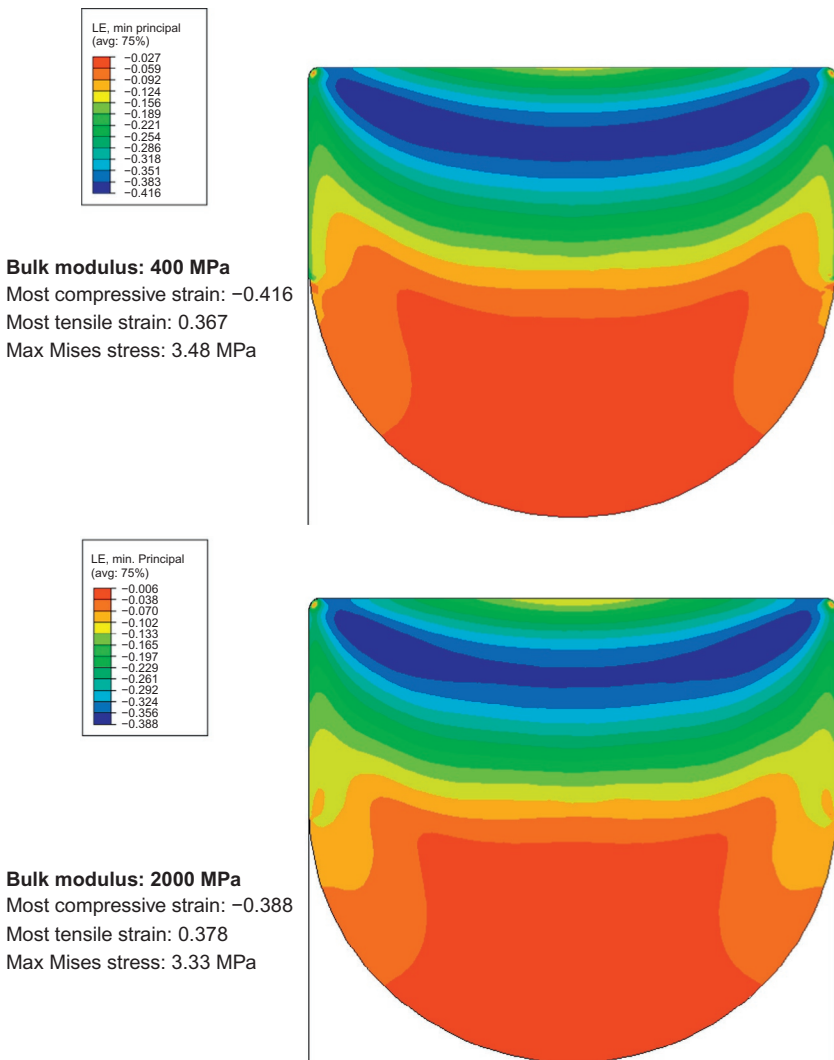


Figure 2.41 Influence of the bulk modulus (and Poisson's ratio) on the predicted response of an o-ring in a confined geometry without a small groove. The predictions were obtained from the BB model.

In small strain volumetric loading, the bulk modulus can be obtained from Hooke's law (see Chapter 5, Section 5.2.1):

$$\kappa = -\frac{P}{\varepsilon_v} = -\frac{\Delta P}{\Delta \varepsilon_v}, \quad (2.9)$$

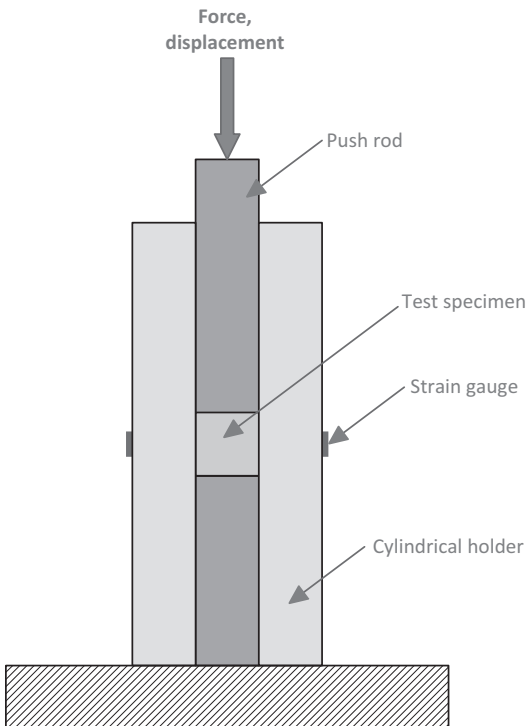


Figure 2.42 Schematic figure of a bulk compression fixture.

where $P = -(\sigma_r + \sigma_\theta + \sigma_z)/3$ is the pressure, and $\varepsilon_v = \varepsilon_r + \varepsilon_\theta + \varepsilon_z$ is the volumetric strain.

In this case, $\varepsilon_r = \varepsilon_\theta = 0$, giving $\varepsilon_v = \varepsilon_z$, and $\kappa = -P/\varepsilon_z$. The axial strain ε_z is given by the applied deformation that is directly measured in the experiment. The experiment also measures the axial stress $\sigma_z = F/A$, but to calculate the bulk modulus it is necessary to know the *pressure*, not only the axial stress.

From Hooke's law with $\varepsilon_r = \varepsilon_\theta = 0$ it directly follows that $\sigma_r = \sigma_\theta$. The radial stress in the specimen can be obtained from the known closed-form solution of a pressurized thick-walled cylinder [23]:

$$\sigma_r = \sigma_\theta^{\text{gauge}} \cdot \frac{b^2 - a^2}{2a^2}, \quad (2.10)$$

where $\sigma_\theta^{\text{gauge}}$ is the circumferential stress from the strain gauge on the outside of the cylindrical holder, b is the outside radius of the cylindrical holder, and a is the radius of the test specimen.

From these equations the pressure can be calculated from:

$$P = -\frac{1}{3} \left[\frac{F}{A_0} + \frac{b^2 - a^2}{a^2} \varepsilon_\theta^{\text{gauge}} E_{\text{holder}} \right], \quad (2.11)$$

where $\varepsilon_\theta^{\text{gauge}}$ is the circumferential strain from the strain gauge and E_{holder} is the Young's modulus of the holder.

One example showing experimental bulk compression data is shown in [Figure 2.43](#). In this case, a cylindrical PTFE specimen was compressed in the confined compression holder. The results from the test show that the initial response consists of a region of low modulus, corresponding to the initial specimen compression until there is full contact with the walls of the fixture. At larger strain, the slope of the pressure-volumetric strain curve gives the real bulk modulus of the material. For this PTFE material the bulk modulus was 2210 MPa.

Like all experimental tests, there are complications also with the bulk compression test. One common way to examine the accuracy of an experimental technique is to perform an FE study of the experimental setup. One example of this approach is shown in [Figures 2.44](#) and [2.45](#).

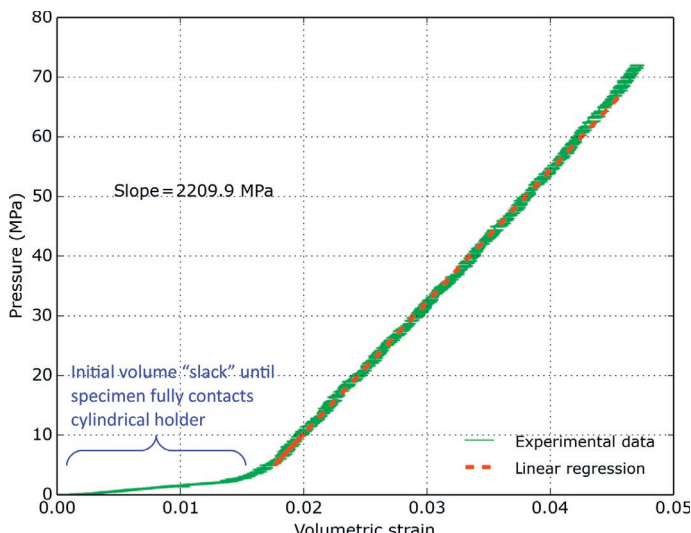


Figure 2.43 Experimental volumetric data for a PTFE material. The slope of the pressure-volumetric strain data is the bulk modulus.

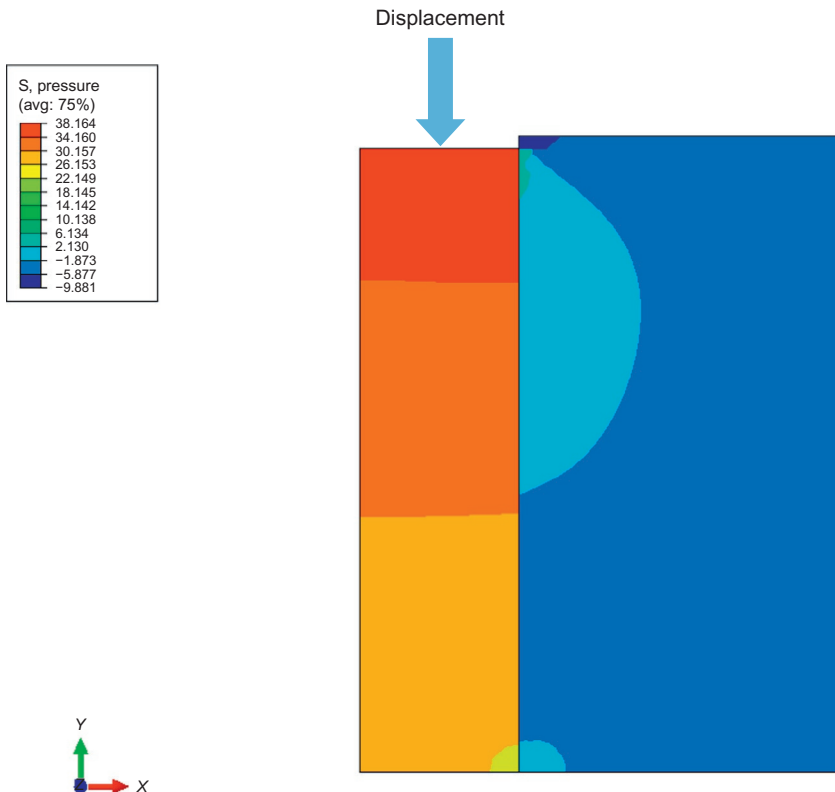


Figure 2.44 FEA predicted distribution of pressure in a volumetrically compressed test specimen. Axisymmetric model of the test.

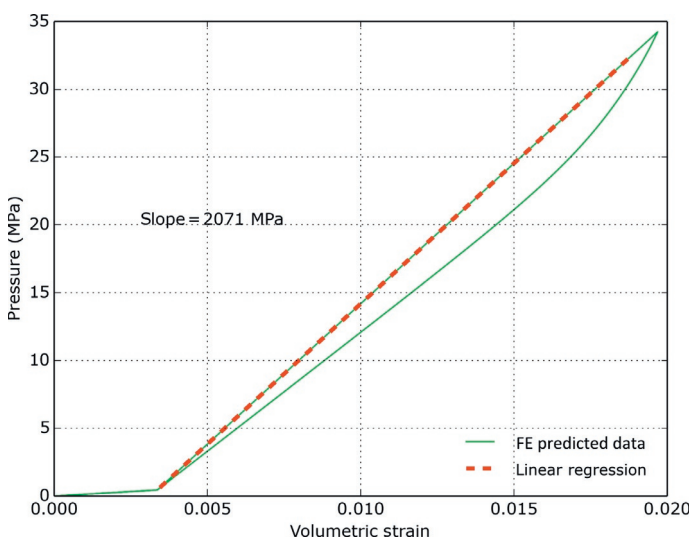


Figure 2.45 FEA predicted pressure-volume response.

In this example, a cylindrical specimen with a diameter of 6 mm and a height of 25 mm was volumetrically compressed in a cylindrical holder with an interior diameter that was just slightly larger than the diameter of the specimen. The specimen was represented using the TN model (see Section 8.6) with a bulk modulus of 2000 MPa. The friction coefficient between the specimen and the cylindrical holder was taken to be 0.05.

[Figure 2.44](#) shows that the pressure distribution becomes inhomogeneous due to the large initial specimen height. Clearly, the lower the friction the more accurate the experiments become.

From the FE simulation the axial force, the applied displacement of the top surface of the specimen, and the strain on the outside surface of specimen holder can be extracted. From this data the pressure and volumetric strain can be calculated from Equation (2.11), see the results plotted in [Figure 2.45](#). The figure shows that the slope of the extracted pressure-volumetric strain data is about 2071 MPa, which is 3.5% higher than the real bulk modulus. It is also interesting to see that there is hysteresis in the pressure-volumetric strain response during cyclic loading. This hysteresis can also be seen in real experimental data.

Further FE analysis shows that the accuracy of this experimental setup can be further improved by using specimens that are less tall, and therefore reduce the influence of frictional forces.

2.2.10 Other Common Mechanical Testing Modes

Other loading modes that are commonly used to determine the stress-strain response of polymers are shown in [Figure 2.46](#). These loading modes include torsion, combined tension-torsion, biaxial tension, 3-pt and 4-pt bending, and confined compression. It is not necessary to use all of these different experimental tests in order to characterize the behavior of a polymeric material.

Depending on what material model is used, it is sometimes recommended to perform tests in uniaxial loading and at least one of the other loading modes. For polymer foams, due to their compressibility, it is important to also run confined compression or triaxial compression in order to separate the shear response

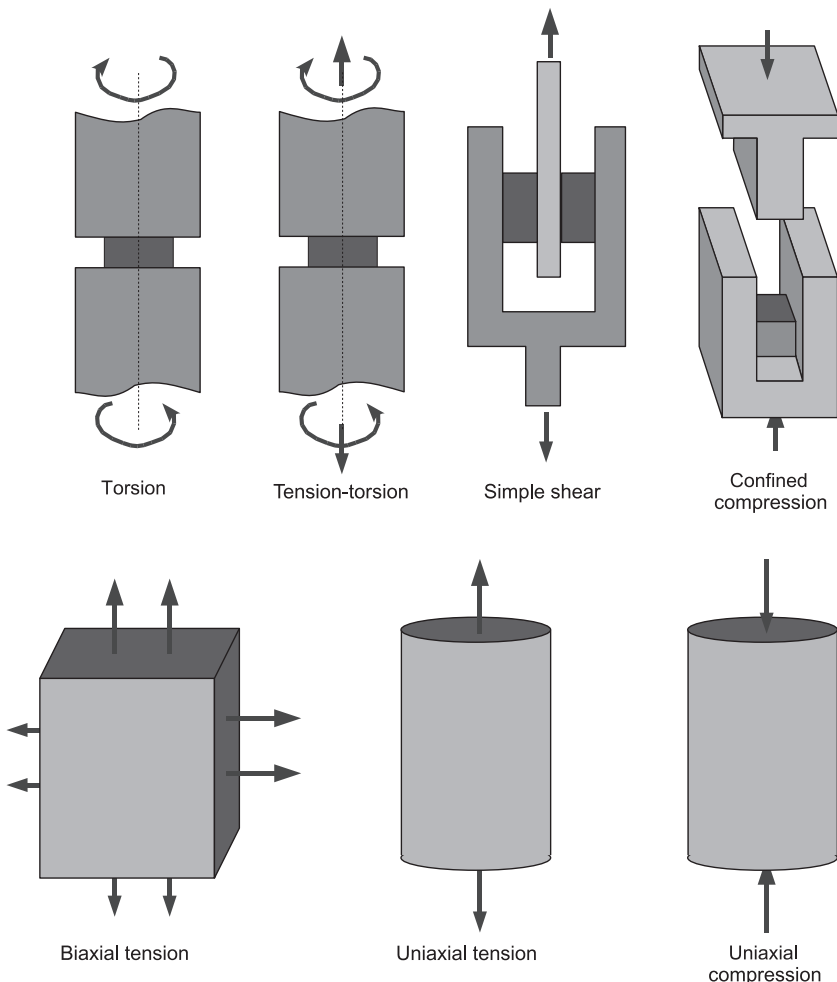


Figure 2.46 Different loading modes that are commonly used for determining the stress-strain response of polymers.

from the volumetric response of the material. The number of different tests and types of loading modes that are required for material model calibration is dependent on the required accuracy of the model predictions and the material model that is chosen. Interestingly, the more advanced material models that are micromechanically motivated (see Chapter 8) typically require fewer loading modes for characterization compared to the purely phenomenological models that often need many different loading

modes for accurate and reliable calibration. The advanced micromechanically motivated models, on the other hand, often need experimental data also for different loading rates and temperatures for calibration.

2.2.11 Testing for Failure Model Calibration

Experimental testing is also critical for calibrating failure models for all types of polymers. This includes fracture mechanics testing, fatigue testing, and damage mechanics testing. In general, the failure testing can be divided into testing of continuum-level failure properties and fracture-mechanics testing. The continuum-level testing is based on the exact testing techniques that have been discussed in the previous sections of this chapter. These tests are either applied in monotonic or cyclic loading to failure depending on the desired type of failure model.

The fracture mechanics testing is performed differently for elastomers and thermoplastics. For elastomers, a number of test geometries have been developed that are particularly useful for determining the critical tearing energy of an elastomer or rubber. [Figure 2.47](#) shows a few common test geometries for this purpose. The Trouser Tear specimen and the Type C Tear specimen are specific specimen geometries for determining the tear strength of rubbers [24], and the compact tension specimen has been developed for measuring the fracture toughness of plastic materials [25].

2.3 Mechanical Testing for Material Model Validation

The previous section introduced a large number of experimental tests that can be used to quantify the mechanical response of a polymer, but the results from those tests can also be used as the source for the selection and calibration of different materials model. Practical aspects of material model calibration is discussed in more detail in Chapter 9.

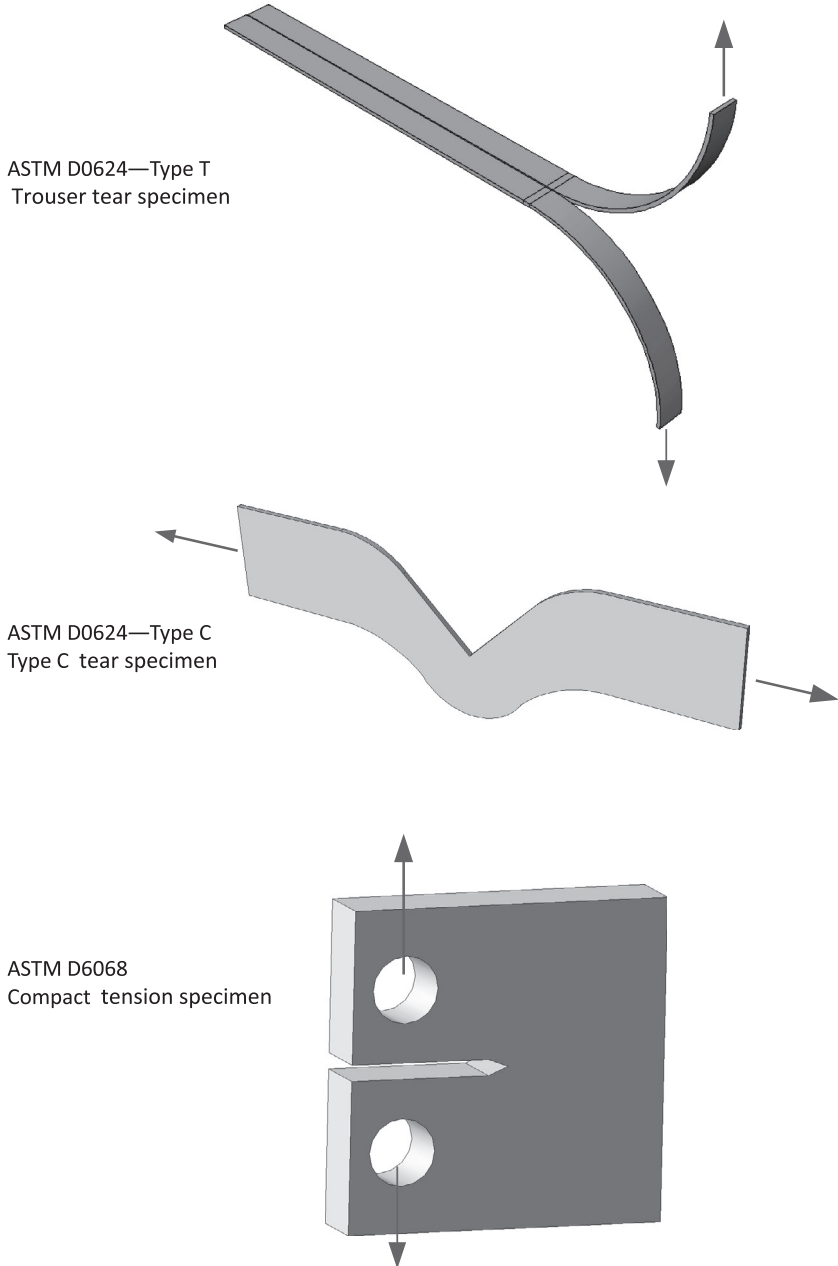


Figure 2.47 Different loading modes that are commonly used for determining the failure response of polymers.

Many times, specifically in industrial settings, the material model calibration is the final step in the material modeling work after which the calibrated material models are inserted into FE input files. This approach is tempting since the end goal is typically the FE analysis of a product or design, or to guide a design optimization. The accuracy of the FE solver is usually excellent as long as the FE mesh is sufficiently fine, but the accuracy of product-level FE results are *not* guaranteed unless suitable and accurate material models have been used. For that reason, it is in general recommended to validate the calibrated material models by comparing FE predictions, that are based on the selected and calibrated material model, to a set of experimental data that was not used for the material model calibration. This new set of experimental data are the *validation test results*. It is typically recommended that the validation tests be performed in a similar loading mode as the intended application, or in a general multiaxial loading mode.

Sometimes the results from an experiment can be used for both material model calibration and material model validation, even if the deformation state in the test specimen is inhomogeneous. If the deformation state is inhomogeneous, then *inverse calibrations* can be used to calibrate the selected material model. Inverse material model calibration is a technique in which an FE simulation is setup of the actual test and the results from that test is then used iteratively as part of the model calibration.

The typical steps that are performed as part of material model validation are shown in [Figure 2.48](#).

2.3.1 Material Model Verification and Validation

Computer simulation models are often used as an important step in product design, problem solving, and used as a tool to provide insight into processes. For this reason it is important to make sure that the simulation models are *verified* and *validated*, in order to make sure the simulation results are as accurate as expected.

Material model *verification* is a process that is used to ensure that the model has been implemented properly with respect to

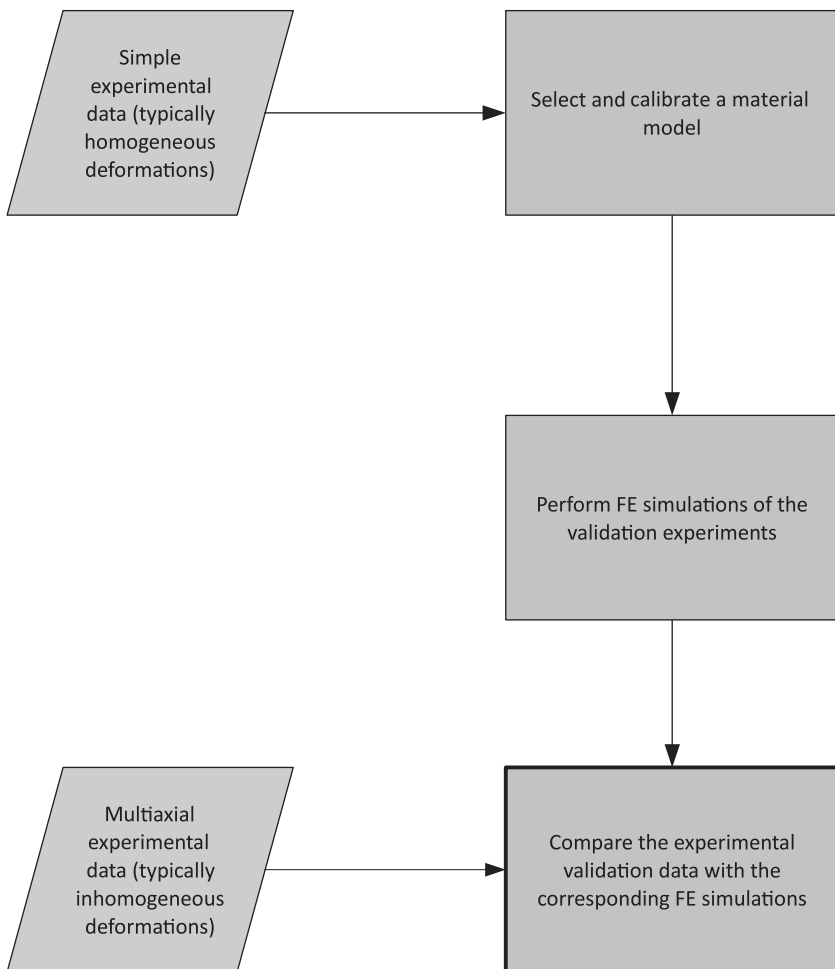


Figure 2.48 Material model validation consists for multiple steps: calibration, multiaxial testing, and validation simulations.

the constitutive equations. This typically include code review, and examining the model predictions from different solution schemes and implementations. Most often this step has been performed by the FE solver provider, or the material model provider. If you are implementing your own material models then you should perform this step very carefully.

Material model *validation* is a process that is used to ensure that the model sufficiently accurately captures the response of a real material. Often validation is limited to a certain range of temperatures and strain-rates.

Material Model Validation:

“Are you using the right material model?”

Material Model Verification:

“Has the material model been implemented right?”

The following sections provide some common experimental tests that can be used for material model validation.

2.3.2 Small Punch Testing

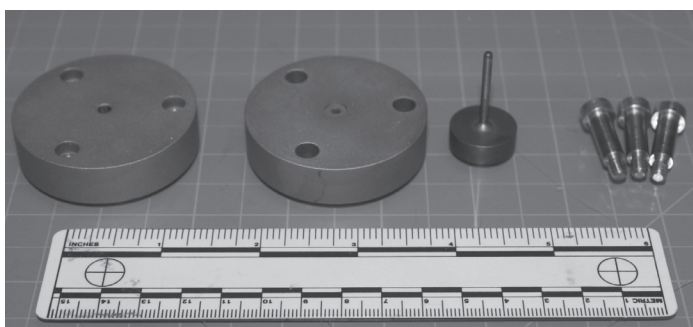
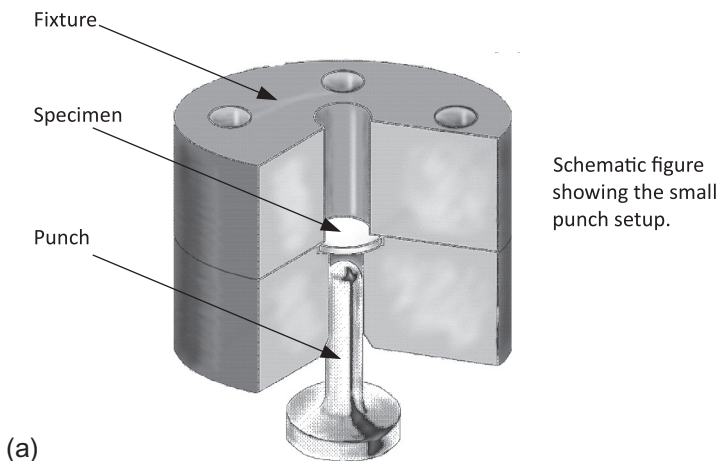
Small punch testing is an experimental technique that can be used to examine the biaxial bending response of thermoplastic and elastomeric materials. The details of the experimental approach is shown in [Figure 2.49](#) and is also described in the ASTM standard F2183 [26]. In this test, a thin cylindrical specimen with a diameter of 6.4 mm and a thickness of 0.5 mm is placed into a steel fixture and then loaded using a hemispherical punch head that drives the specimen to deform in a loading mode similar to biaxial drawing, see [Figure 2.50](#). During the test the force-displacement response of the punch head is measured.

The main benefit of this test is that can be performed on small specimens that can be extracted from, for example, retrieved medical devices [27–29]. Since the experimental test is easy to perform and since it introduces a multiaxial stress and strain state in the material, it is also a useful material model validation test. Validation testing is discussed in more detail in [Section 2.3](#).

The small punch test is easy to analyze using FE simulations. [Figure 2.50](#) shows an exemplar axisymmetric FE mesh of a small punch specimen.

The main challenge with the small punch test is the strong influence of friction. [Figure 2.51](#) shows the results from a case study in which three friction coefficients were examined (0, 0.1, and 0.2). The figure shows that at large deformations the force-displacement response can be rather strongly dependent on the friction coefficient.

The table below shows how the friction coefficient influence the max stress, max strain, and the minimum specimen thickness.



(b) Photograph of a disassembled small punch fixture .

Figure 2.49 Schematic figure of a small punch fixture. (Reproduced with permission from Veryst Engineering, www.veryst.com.)

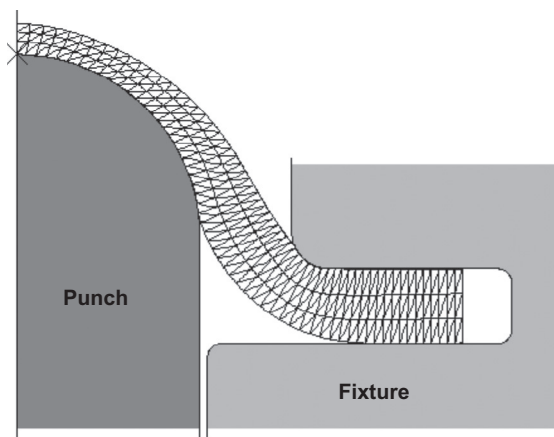


Figure 2.50 Schematic FE mesh of a small punch specimen being loaded by a hemispherical punch head.

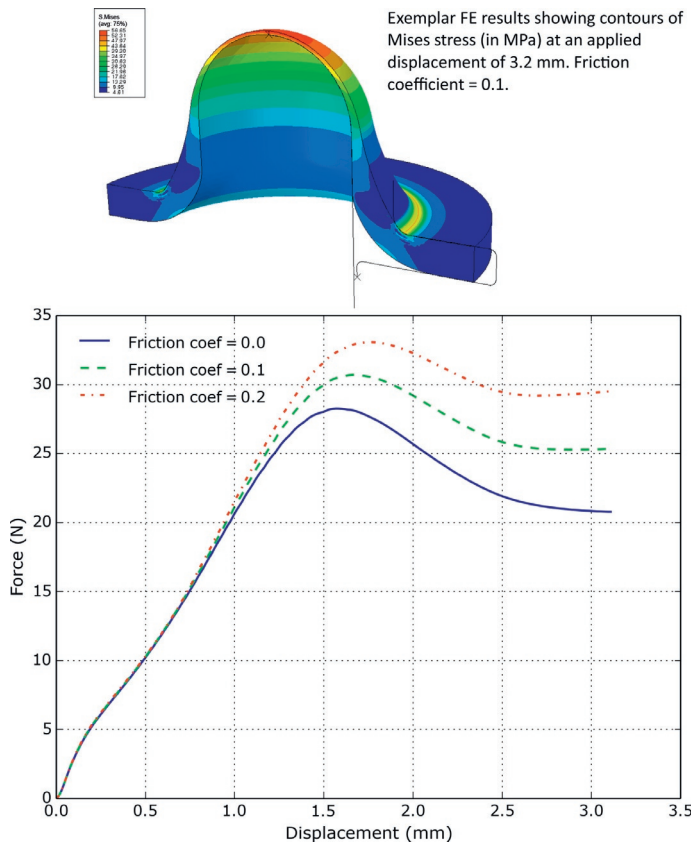


Figure 2.51 Results from an FE study of the influence of friction on the small punch results.

These results clearly show that at large punch displacements all stress and strain fields in the specimen are strongly dependent on the friction coefficient. Hence, in order to effectively use this multiaxial test it is important to have a good understanding of the friction coefficient between the test specimen and the steel material in the fixture.

Friction Coefficient	Max Mises Stress (MPa)	Max Principal Strain	Min Thickness (mm)
0	76.5	1.41	0.47
0.1	56.7	1.22	0.45
0.2	45.3	1.09	0.43

2.3.3 V-Notch Shear Testing

V-notch shear is another common experimental method for examining the multiaxial stress and strain response of a polymer. The V-notch shear is an attractive method since it mainly probes the shear behavior, and it does not suffer from uncertainties due to friction. This experimental method is also called *Iosipescu Shear* and described in ASTM D5379 [30]. A photograph of the shear fixture is shown in Figure 2.52.

The stress field in the V-notch specimen can be examined using an FE study. Figure 2.53 shows one example where a specimen modeled using the TN model with material parameters suitable for UHMWPE.

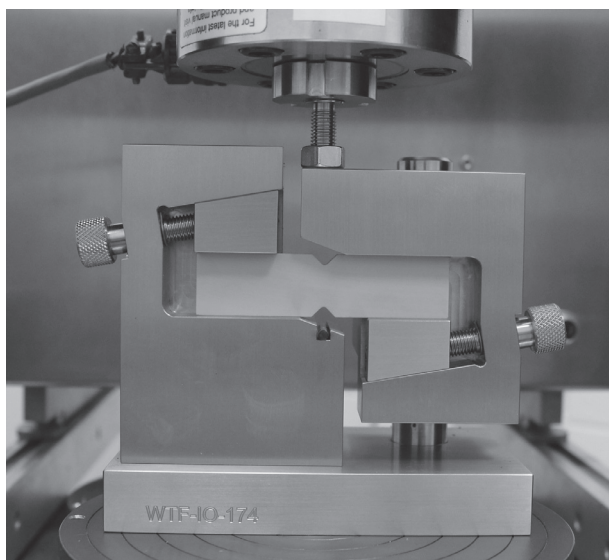


Figure 2.52 Photograph of a V-notch shear fixture. (Reproduced with permission from Veryst Engineering, www.veryst.com.)

2.4 Surface Characterization Techniques

There are numerous experimental techniques that can be used for characterizing surface topology, structure, and chemistry of

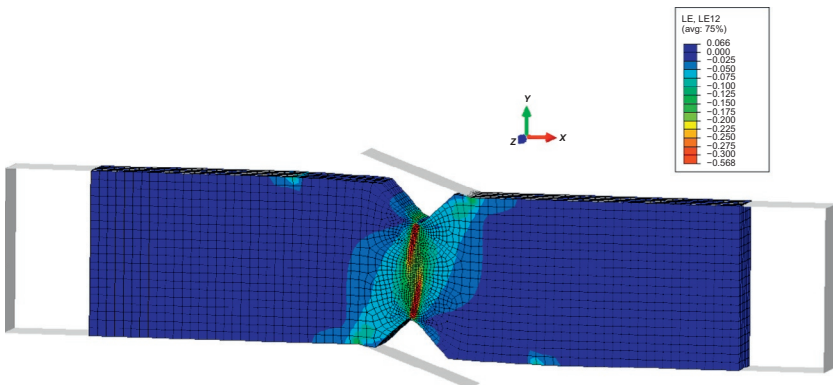


Figure 2.53 Predicted distribution of shear strain in the V-notch shear test.

polymers. The most important and commonly used techniques are reviewed in the following sections.

2.4.1 Optical Microscopy

Optical microscopes are designed to create magnified visual or photographic images of small objects. To accomplish this, the microscope is designed to perform three tasks: create a magnified image of the sample, distinguish different details of the image, and make the final image visible to the human eye or camera. This class of characterization instruments includes everything from a simple magnifying glass to advanced multi-lens microscopes.

There are two basic ways in which optical microscopes can be operated depending on how the light is projected on the sample. The first approach, which is widely used to study biological polymers, is to prepare very thin specimens and have the light transmit through the sample. The second approach is used for thicker-section samples and nontransparent materials. Here, the light passes through the objective and then reflects from the surface of the sample and into the microscope objective. These two techniques are referred to as *transmitted* and *reflected light microscopy*.

The resolution limit of optical microscopes is controlled by diffraction, which in turn is controlled by the numerical aperture

(A_N) of the optical system and the wavelength of the light used (λ). Assuming that optical aberrations are negligible, the resolution (d) is given by:

$$d = \frac{\lambda}{A_N}. \quad (2.12)$$

By assuming $\lambda = 550$ nm (corresponding to green light), and $A_N = 1.5$ (corresponding to oil as a medium), the maximum resolution becomes about $0.3 \mu\text{m}$. One of the main drawbacks of optical microscopy is this relatively large resolution limit.

Another limitation of optical microscopy is the poor contrast produced when light is passed through very thin specimens or reflected from surfaces with a high degree of reflectivity. Different optical techniques have been developed to improve the contrast of optical microscopy. Some of the more important and commonly used techniques are: polarized light, phase contrast imaging, differential interference contrast, fluorescence illumination, dark-field illumination, Rheinberg illumination, Hoffman modulation contrast, and the use of various gelatin optical filters. Some of these techniques are briefly discussed in the following. A more detailed discussion of these and other optical microscopy techniques are given in [31, 32].

- **Polarized Light Microscopy**

This technique uses optical anisotropy to reveal the structure of the sample. The microscope is equipped with a polarizer and an analyzer. The enhanced contrast results from interaction of the plane-polarized light with a birefringent specimen (doubly refracting) to create two perpendicular optical waves. Due to the interaction with the specimen, the velocities of the two waves are different, causing the two waves to be out of phase. The light components are combined with interference as they pass through the analyzer. This technique can enhance the contract and quality of the final image.

- **Darkfield Microscopy**

By using specialized oblique illumination, the contrast can be improved of specimens that are normally not well captured using brightfield illumination. In the optical equipment, the direct light is stopped by an opaque block in the condenser, but light from oblique angles at all azimuths passing through the specimen are reflected, refracted, and diffracted into the microscope objective, creating a high contrast image with a dark background.

- **Differential Interference Contrast**

Differential interference contrast microscopy is a beam-shearing interference system in which the reference beam is sheared by a very small amount. The technique creates a shadow-cast image that increases contrast from the gradient of optical paths for both high and low spatial frequencies present in the specimen.

- **Confocal Microscopy**

Confocal microscopy is a new interesting technique that has the ability to control the depth of field, and collect serial optical sections from thick specimens. The approach is to use spatial filtering to remove out-of-focus light. The technique can be used to create very high-quality images and has become an important tool for optical microscopy.

- **Near-Field Scanning Optical Microscopy**

Near-field scanning optical microscopy (NSOM) can be used to create ultra-high optical resolution. To get the high resolution a sub-micron optical probe, positioned very close to the sample, transmits light through a small aperture. The region within a single wavelength from the specimen surface is defined as the near-field. Within this region, evanescent light is not diffraction limited and nanometer resolution can be obtained.

- **Fluorescence Microscopy**

Fluorescence microscopy is primarily used with episcopic illumination and is rapidly becoming a standard tool in the fields of genetics, and cell biology.

- **Stereo Microscopy**

Stereo microscopes have a different design than traditional microscopes. It uses two eyepieces (or sometimes two complete microscopes) to provide slightly different viewing angles to the left and right eyes. This produces a three-dimensional (3D) visualization of the sample being examined. The stereo microscope is often used to study the surfaces of solid polymers or investigate fracture surfaces.

2.4.2 Scanning Electron Microscopy

Scanning electron microscopy (SEM) is one of the most important surface characterization techniques that is used today. One of the major advantages of SEM is the great depth of field. In addition, SEM equipment are often coupled with energy dispersive spectroscopy (EDS) X-ray diffraction, see [Section 2.6.2](#), thereby enabling both high magnification characterization of surfaces and elemental composition analysis.

The scanning electron microscope uses electrons rather than light to form an image. This enables a larger depth of field, which allows a larger amount of the sample to be in focus at one time. The SEM also produces images of high resolution. Preparation of the samples is relatively easy since most SEMs only require the sample to be conductive. For polymers this can be achieved, for example, by gold coating the sample. The combination of higher magnification, larger depth of focus, greater resolution, and ease of sample observation makes the SEM one of the most heavily used instruments in experimental materials characterization.

In a typical SEM setup, electrons are emitted from a cathode filament toward an anode. The electron beam, which is typically

given an energy ranging from a few keV up to 50 keV, is focused by condenser lenses into a beam with a very fine spot size (about 5 nm). The electron beam then passes through the objective lens, and scanning coils which deflect the beam in a desired pattern on the sample surface. When the primary electrons reach the surface they are inelastically scattered by atoms in the sample. These scattering events cause the primary beam to spread and create emission of electrons and X-rays, which are then detected and used to produce an image of the surface.

In the most common imaging mode, low energy secondary electrons are detected by a scintillator-photomultiplier component and the resulting signal is used to create an image of the sample. Because the secondary electrons come from within 1 nm of the surface, the brightness of the signal depends on the surface area that is exposed to the primary beam. This surface area is relatively small for a flat surface, but increases for steep surfaces. Thus steep surface and edges (cliffs) tend to be brighter than flat surfaces resulting in images with good 3D contrast. Using this technique, resolutions of the order of 5 nm are possible.

Another mode to operate an SEM is to detect backscattered electrons which are essentially elastically scattered primary electrons. Backscattered electrons may be used to detect both topographical and compositional detail, although due to their much higher energy (approximately the same as the primary beam) these electrons may be scattered from fairly deep within the sample. This results in less topological contrast than for the case of secondary electrons. However, the probability of backscattering is a weak function of atomic number, thus some contrast between areas with different chemical compositions can be observed especially when the average atomic number of the different regions is quite different.

The spatial resolution of the SEM is controlled by the size of the spot of the electron beam, and the size of the material which interacts with the electron beam. Since these are larger than the interaction distance it is not possible to image atomic scale images.

A new surface characterization technique is *environmental SEM* (ESEM). This approach works with controlled environmental conditions and requires no conductive coating on the specimen. This enables studies of specimens in their natural state. The environment in an ESEM can be selected from among water vapor, air, N₂, Ar, O₂, etc. Dynamic characterization of wetting, drying, absorption, melting, corrosion, and crystallization can be performed using ESEM.

ESEMs are able to work with certain pressures and without surface charging because the secondary electron detector is designed on the principle of gas ionization. As primary electrons are emitted from the gun system, the secondary electrons on the specimen surface are accelerated toward the detector, which is biased by a moderate electric field. The collisions between the electrons and gas molecules liberate more free electrons, and thereby provide more signals. Positive ions created in the gas effectively neutralize the excess electron charge built up on the specimen.

One exemplar SEM image is shown in Figure 2.54. This figure shows the topology and structure of Tin oxide particles on a polyetherimide (PEI) substrate. The bar in the legend of the figure is 10 μm long.

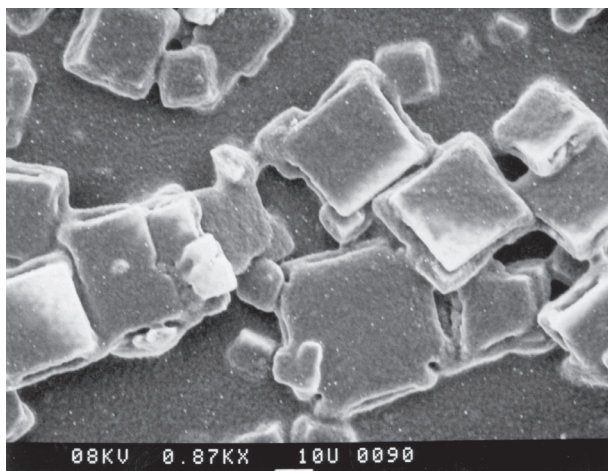


Figure 2.54 Exemplar SEM image showing Tin oxide particles on a PEI substrate.

2.4.3 Atomic Force Microscopy

The atomic force microscope (AFM) is a powerful high magnification microscope that was developed by Binnig, Quate, and Gerber in 1986 [33]. The AFM uses a cantilever with a sharp tip to study surface features. During operation the cantilever tip is brought into close proximity of the sample surface. The force from the sample on the cantilever beam causes a deflection of the cantilever beam tip, and this deflection is measured using laser techniques. Unlike traditional microscopes, AFM does not use lenses, hence the size of the probe tip rather than diffraction typically control the experimental resolution.

The AFM typically operate in one of two modes: (1) contacting mode with the tip contacting the specimen and (2) noncontacting or tapping mode. In contacting mode, the specimen is mounted on a piezoelectric crystal and the cantilever deflection is monitored in order to keep the distance between the probe tip and the sample constant. The tip is then scanned across the specimen surface and the vertical displacement necessary to maintain a constant force on the tip is recorded. The resulting height map represents the topography of the specimen surface ([Figure 2.55](#)).

In noncontacting or tapping mode, the cantilever is externally oscillated close to its resonance frequency. The vibration characteristics of the cantilever beam is influenced by the tip-sample interaction forces; these changes in oscillation provide information about the specimen geometry. One of the main advantages of the dynamic mode is that it generates lower lateral forces on the sample, and it is therefore widely used to image biological samples.

The noncontacting dynamic mode can be run using frequency modulation, or more commonly amplitude modulation. In amplitude modulation, changes in the oscillation amplitude yield topographic information about the sample. Additionally, changes in the phase of oscillation under tapping mode can be used to discriminate between different types of materials on the surface.

The AFM has several advantages over electron microscopy. One is that it provides a true 3D surface profile. Additionally,

samples viewed by an AFM do not require any special treatment that can destroy the sample and prevent its reuse. While an electron microscope needs a vacuum environment for proper operation, the AFM can be used also in an ambient or even liquid environment.

The main disadvantage of the AFM compared with the SEM is the image size. The SEM can show image representations of a few mm^2 area and a depth of field of a few mm. The AFM, on the other hand, can only show a maximum area of about 0.01 mm^2 with a max depth of field of a few μm .

Another common use of AFM is to measure the indentation resistance and stiffness of a specimen by measuring the force required to depress the probe tip a small distance into the specimen. In addition to this indentation-type test, AFM are commonly used also in the following applications:

- Examine dispersion and particle size of additives in polymer matrix.
- Study phases of blends and alloys.
- Image and quantify surface texture or roughness (topography).

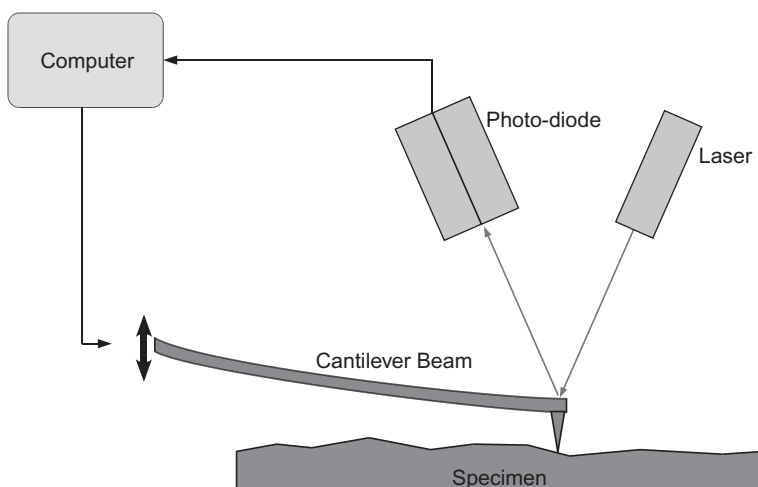


Figure 2.55 Schematic view of an AFM.

2.5 Volume Characterization Techniques

There are numerous experimental techniques that can be used to study the bulk properties of polymers. These volume characterization techniques are typically very different from the surface characterization techniques that were discussed in the previous section. The most common volume characterization techniques are discussed in the following sections.

2.5.1 Differential Scanning Calorimetry

Differential scanning calorimetry (DSC) is a commonly used technique for analyzing thermal transitions in polymers and other materials. It provides information about the temperatures at which transitions occur as well as quantitative measurements of the heat transitions associated with the events.

All materials that undergo a change in physical state (e.g., recrystallization or melting), or undergo a chemical reaction, will release absorbed energy as part of the transition. A differential scanning calorimeter is designed to measure the enthalpy changes that occur during these transitions. In the experimental setup, both the test specimen and a reference sample are heated at a predefined temperature rate and the differential heat flow required to maintain the sample at the same temperature as the inert reference specimen is measured.

Results from a typical DSC run are shown in [Figure 2.56](#). In this experiment, a small sample (about 10 mm^3) was heated at a rate of $20\text{ }^\circ\text{C/min}$. The figure shows the input heat flow that was required to maintain the prescribed temperature history. The graph provides direct information about the glass transition temperature (T_g), the exotherm associated with crystallization, and the endotherm associated with melting.

DSC can also be used to study the influence of mechanical deformation and residual stresses on the required heat flow for the thermal transitions [34]. By coupling mechanical testing and thermal pretreatments it is possible to explore the micromechanisms controlling the activation energy for local rearrangements.

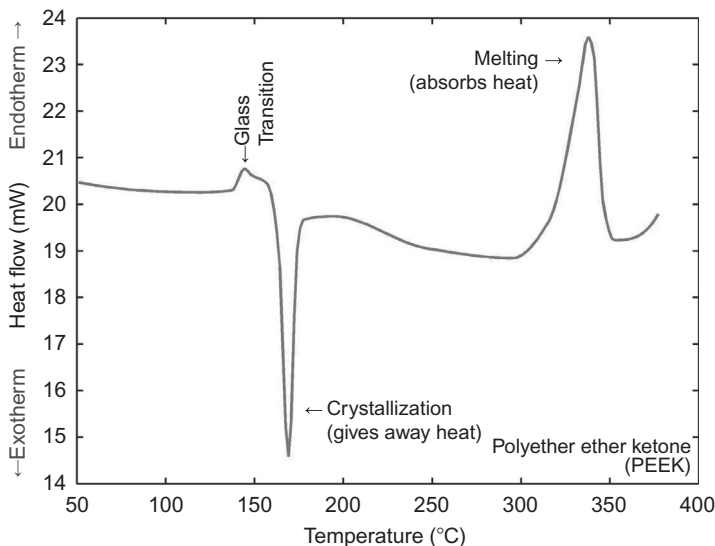


Figure 2.56 Exemplar DSC scan of PEEK showing the glass transition temperature, the crystallization peak, and the endotherm during melting.

This method can provide valuable information about the processes that must be accounted for in the development of accurate constitutive models for the material behavior.

2.5.2 Transmission Electron Microscopy

Transmission electron microscopy (TEM) is a powerful technique that can produce higher magnification than what can be achieved by SEM. One of the main limitation of TEM is that the test specimen must be a foil so thin that an electron beam can pass through it. In addition, the specimen must be able to withstand the high vacuum inside the TEM instrument. Because of these requirements, most materials studied with TEM are of inorganic, nonbiological materials.

The TEM is widely used in materials science and metallurgy, and for the study of crystalline materials such as metals and semiconductors, but is also very useful for studies of filler morphology in polymers. One example of this is shown in [Figure 2.57](#)

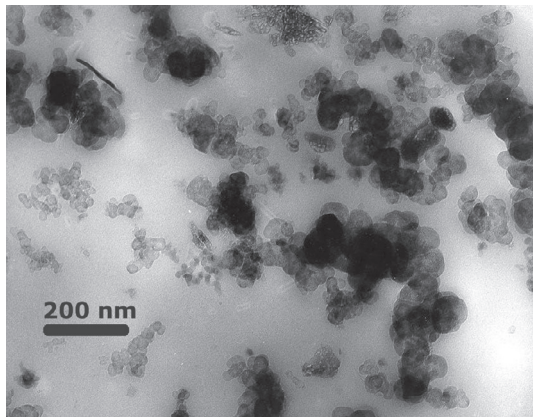


Figure 2.57 TEM of CR with 7 vol% CB [35].

illustrating a chloroprene rubber (CR) filled with 7 vol% N600 carbon black (CB). The black regions in the figure are the carbon black particles. The micrograph shows that the particles have a spherical shape with a diameter of 20 nm, and that the carbon black particles have a tendency to cluster together into larger aggregates.

The contrast in a TEM image is different from the contrast in a light microscope image. A crystalline material interacts with the electron beam mostly by diffraction rather than absorption. If the planes of atoms in a crystal are aligned at certain angles to the electron beam, the beam is transmitted strongly; while at other angles, the beam is diffracted, sending electrons in another direction. In the TEM, the specimen holder allows the user to rotate the specimen to any angle in order to establish the desired diffraction conditions.

In the most powerful diffraction contrast TEM instruments, it is possible to produce a diffraction pattern image which is directly analogous to the planes of atoms in the crystal. Although the way contrast arises in these atomic-resolution images is complex, and such images are often interpreted using computer modeling of the electron beam and magnetic lenses, these images have added a new layer of understanding to the study of crystalline polymer materials.

2.5.3 X-Ray Diffraction

X-ray diffraction is an important tool for studying both amorphous and semi-crystalline polymers [36, 37]. It can be used to analyze many features of the microstructure of the material, including lattice parameters, presence of imperfections, crystallographic orientations (texture), and degree of crystallinity.

In a typical X-ray diffraction experiment, the polymer sample is exposed to X-ray radiation which is a form of electromagnetic radiation with a short wave length ($\lambda \approx 0.1$ nm). The X-ray radiation is often produced by bombarding a metal target with fast electrons in a vacuum tube. When created this way, the radiation often consists of two components: a continuous spectrum of white radiation, and a superimposed line spectrum having a frequency that depends on the metal being bombarded. When the X-ray beam transverses through the specimen it loses its intensity exponentially: $I = I_0 \exp(-\mu x)$, where I_0 is the initial intensity and μ is a linear absorption constant. Hence, the depth of X-ray penetration depends on the material and the energy of the X-ray source.

The incident beam of X-rays is partly absorbed, partly scattered, and the rest is transmitted unmodified through the specimen. The scattering occurs due to interaction between the incident X-ray beam with the electrons in the material, and the diffracted X-rays interact with each other to cause diffraction patterns that depend on the angle of the incident beam in relation to the specimen orientation. In this context, the words scattering and diffraction are used interchangeably.

X-ray diffraction can also be used to study amorphous polymers. The diffraction pattern from amorphous polymers is lacking sharp peaks that are characteristic of crystals, and instead consists of broad features. Quantitative diffraction analysis of amorphous polymers can provide important information about the local atomic structure, including bond lengths, morphology, and radial distribution information.

X-ray diffraction techniques are often categorized as wide-angle X-ray scattering (WAXS) and small-angle X-ray scattering

(SAXS). WAXS is typically used to study structures with a length scale of about 1 nm, and SAXS is used to study larger features with a length scale of 1 nm to about 400 nm.

Wide-Angle X-Ray Diffraction

The principle of wide-angle X-ray diffraction can be exemplified by considering a beam of X-rays with a wavelength λ impinging at an angle θ on a diffracting material with a set of crystal planes of spacing d , see Figure 2.58.

A diffracted X-ray beam at the angle θ will only exist if the rays from each successive lattice plane reinforce each other. For this to occur, the extra distance a ray has to travel must be equal to an integral number of wavelengths, $n\lambda$. This is expressed in the well-known Bragg law:

$$n\lambda = 2d \sin \theta, \quad (2.13)$$

where n is an integer, λ is the wavelength of the X-ray beam, d is the lattice spacing, and θ is the angle between the lattice planes and the incident beam.

To ensure that Bragg's law is satisfied and that reflections from various crystal planes can occur, it is necessary to provide a range of either θ or λ . The two most common methods to achieve this are the *Laue method* and the *powder method*.

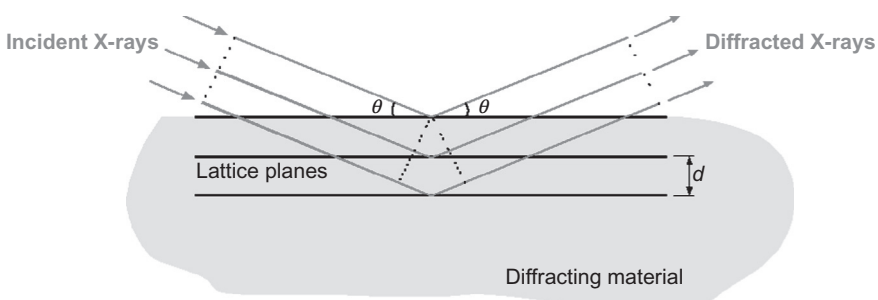


Figure 2.58 Wide-angle X-ray diffraction from crystal planes.

- In the *Laue method*, a stationary crystal is exposed to a beam of white radiation. Since a range of wave lengths is provided, each set of lattice planes will chose the appropriate λ to give Bragg reflection. The resulting refraction pattern can be used to obtain information about the crystalline structure.
- In the *powder method*, monochromatic radiation is used to bombard a finely powdered (or fine-grained) wire of the material. In this case, the Bragg angle θ is variable and crystals with the appropriate orientation will give Bragg refraction.

One example of an X-ray diffraction intensity plot is shown in [Figure 2.59](#). The figure shows the scattering intensity as a function scattering angle for a polyethylene. The measured intensity consists of a Bragg diffraction peak from the crystalline phase superimposed on the diffuse scattering from the amorphous phase. By separating the contributions from the amorphous and crystalline phases it is possible to determine the degree of crystallinity of the material [38].

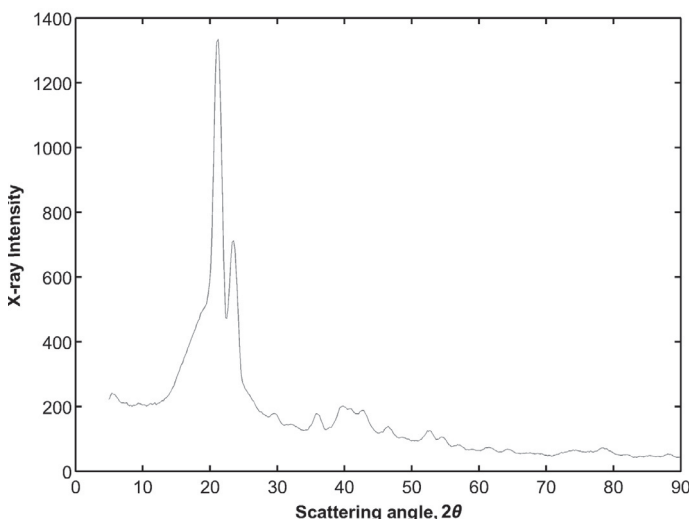


Figure 2.59 Detected X-ray intensity as a function of scattering angle for polyethylene.

Small-Angle X-Ray Diffraction

Small angle X-ray diffraction is a useful technique for studying structural features with a size between 1 nm and about 400 nm. In a common experimental setup, the X-ray radiation is created using a Cu $K\alpha$ emission line with a wavelength of $\lambda = 0.154$ nm giving $\theta = 4.4^\circ\text{C}$ and $\theta = 0.04^\circ\text{C}$, for $d = 1$ nm and $d = 100$ nm, respectively.

The experimental setup is similar to what is used for WAXS, but since the scattering beam is so close to the unmodified transmitted beam it is often required to use a specialized experimental setup that collimates that incident beam very precisely.

The X-ray diffraction patterns can be determined by measuring the intensity of the scattered X-rays as a function of scattering direction. By studying the diffraction pattern it is possible to, for example, examine individual crystal defects by determining any differences in refracted intensity near the defect.

2.5.4 Birefringence

Birefringence spectroscopy is an optical technique that can be used to determine molecular orientation in a polymer sample by measuring the retardation of polarized light passing through the sample [39]. The experimental technique is based on the difference in refractive indexes, n_i , in different directions of the specimen:

$$n_i = \frac{\text{Speed of light in vacuum}}{\text{Speed of light in direction } i \text{ in the sample}}. \quad (2.14)$$

The refractive index for a polymer in a given direction is depending on the polarizability of the molecular bonds and the directional distribution of the macromolecules. For most polymers the refractive index parallel to the main chain encounters primarily C–C bonds, which have low polarizability and hence a refractive index close to 1. In a direction perpendicular to the molecular backbone, many polymers have side-groups that retard the light more creating a higher refractive index.

Birefringence Δn is the difference in the refractive indexes of two perpendicular directions in a material: $\Delta n = n_1 - n_2$. A polymer sample will have a nonzero birefringence if two conditions are satisfied:

1. *On the molecular scale there must be a finite difference in refractive indexes in different directions.* Virtually all polymers satisfy this condition due to the inherent anisotropic nature of the repeat unit.
2. *On the macroscale there must be an anisotropic orientation of the macromolecules.* Hence, if the molecular chains are randomly oriented then the different refractive indexes will cancel each other out and the birefringence will be zero.

The total birefringence of a polymer specimen is controlled by sum of the polarizability of all molecular chains. This connection between birefringence and molecular orientation is what makes this experimental technique interesting. A common experimental study is to measure the amount of birefringence as a function of applied stress and strain. Since the molecular chains are stretching and rotating during an applied macroscopic deformation, birefringence measurements during deformation can provide interesting insight into these molecular events.

As will be discussed in Chapter 5, a number of different molecular chain models have been developed. These models are used, for example, when developing hyperelastic models of rubbers as they describe the orientation of the individual segments of the molecular chains as a function of applied strain. These theoretical expressions can be used together with statistical methods to derive the birefringence as a function of applied load or deformation. Hence, birefringence can also be a useful tool for the development and validation of micromechanism inspired constitutive models.

Birefringence is also often used to study: molecular defects in polymeric solids, thermal strains and residual stresses, and morphological and structural changes. Birefringence can be used

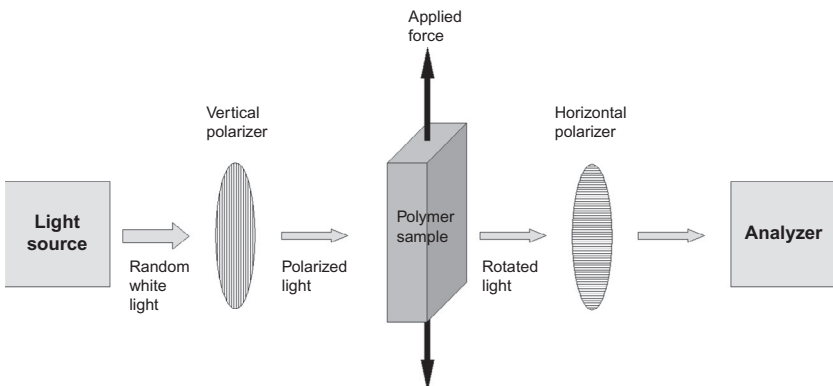


Figure 2.60 Experimental setup used for measuring birefringence.

to study everything from a single polymer chain subject to a flow field, amorphous polymers, semicrystalline polymers, and block copolymers.

Birefringence in the solid state is often called strain birefringence, and birefringence in a liquid state is often called flow birefringence. Birefringence experiments are typically performed by uniaxially deforming a thin sample and measuring the difference in refractive indexes between the deformation direction and a lateral direction, see [Figure 2.60](#).

The birefringence of many polymer systems at small to moderate deformations is found to follow the *stress-optical rule* SOR: $\Delta n = C\sigma$, where Δn is the birefringence, σ is the tensile stress, and C is the stress-optical constant, see [Figure 2.61](#).

As is shown in this figure, glassy polymers do not follow the stress-optical rule (SOR) even at small strains, whereas elastomers typically follow the SOR at small strains but start to deviate at the onset of strain-induced crystallization.

2.5.5 Swell Testing

If a crosslinked polymer is immersed in a good solvent it will swell. The crosslinks in the material will keep the macromolecular structure intact and the material will not dissolve. The equilibrium amount of swelling is controlled by the elastic forces

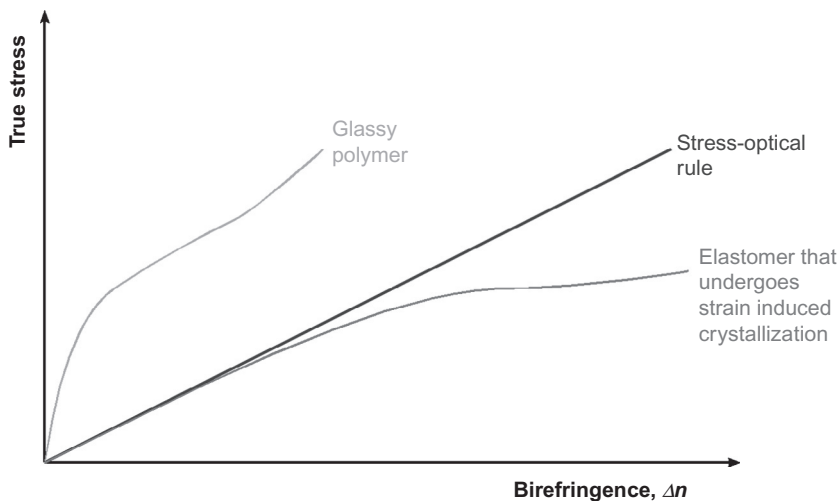


Figure 2.61 Illustration of stress-birefringence relationship for a stretching process of different types of polymers.

from molecular stretching that resist the swelling, and the forces derived from the free energy of mixing. The equilibrium amount of swelling can be used to determine the gel content, crosslink density, molecular weight between crosslinks, and the number of repeat units between crosslinks. These terms can be defined as follows:

- g , gel content—the mass percentage of polymer insoluble in a specific solvent after extraction.
- v_d , crosslink density—the average number of crosslinks per unit volume.
- M_c , molecular weight between crosslinks—average molecular weight between crosslinks.
- q_s , swell ratio—ratio of equilibrium volume in a swollen state to the initial volume.

There are two common techniques that can be used to study the swell ratio of crosslinked polymers: gravimetric measurements [40] and continuous height measurement during swelling [41].

In the gravimetric approach, specimens of the crosslinked plastic are weighted and then immersed in the solvent at a specified temperature for a specified time. After the solvent exposure the specimens are removed, dried, and reweighed. The amount of material extracted and the swell ratio is calculated from these weight measurements. The percent extracted is a measure of the amount of polymer that is soluble and not attached to the main gel phase.

In the height measurement approach, the change in specimen height is measured as a function of exposure time to the solvent at a given temperature. From the results from this experiment the swell ratio can be directly obtained from:

$$q_s = \frac{\text{Final volume}}{\text{Initial volume}}. \quad (2.15)$$

If the Flory interaction parameter ξ for the polymer-solvent system is known, then Flory's network theory [42] can be used to determine the crosslink density and the molecular weight between crosslinks can be determined from the steady-state swell ratio [41].

Swell testing experiments are useful for both quality control and for quantitative network studies. Since the amount of equilibrium swelling is sensitive to type of solvent and the test temperature, it is recommended that one of the applicable standards be followed.

2.6 Chemical Characterization Techniques

Most chemical characterization techniques are based on spectroscopy—the study of spectra—and how a physical property depend on frequency. Spectroscopy is used for the identification of substances, through the spectrum emitted or absorbed. Different spectroscopy techniques are classified according to the physical quantity which is measured or calculated, or the measurement process.

There are two main types of spectroscopy. The first is absorption spectroscopy which uses the range of electromagnetic spectra

in which a substance absorbs. The sample is vaporized and then light of a particular frequency is passed through the vapor. The amount of absorption can be related to the chemical composition of the material. The second type is emission spectroscopy which uses the range of electromagnetic spectra in which a substance radiates. It requires the substance to be vaporized at high temperatures by placing it in a spark gap.

Spectroscopy is often used in combination with chromatography, which is a broad range of physical methods used to separate and/or to analyze complex mixtures. The components to be separated are distributed between two phases: a stationary phase bed and a mobile phase which percolates through the stationary bed. These two techniques, and methods based on them, are discussed in more detail in the following sections.

2.6.1 Fourier Transform Infrared Spectroscopy

Fourier transform infrared spectroscopy (FTIR) is an analytical technique used to identify organic (and in some cases inorganic) materials, including polymer compounds. This technique measures the absorption of various infrared light wavelengths by the material of interest. These infrared absorption bands identify specific molecular components and structures. Fourier transform spectroscopy is more sensitive and has a much shorter sampling time than conventional spectroscopic techniques.

In a conventional spectrometer, a sample is exposed to electromagnetic radiation and the responding intensity of transmitted radiation is monitored. The energy of the radiation is varied over the desired range and the response is plotted as a function of radiation energy (or frequency). At certain resonant frequencies characteristic of the specific sample, the radiation will be absorbed resulting in a series of peaks in the spectrum, which can then be used to identify the sample.

In Fourier transform spectroscopy, the sample is exposed to a single pulse of radiation. The resulting signal, called a free induction decay, contains a rapidly decaying signal of all possible

frequencies. Due to resonance in the sample, certain resonant frequencies will be dominant in the signal and by applying a Fourier transform to the response signal the frequency spectrum can be calculated. Using this approach the Fourier transform spectrometer can produce the same kind of spectrum as a conventional spectrometer, but in a much shorter time.

Absorption bands in the range of 4000-1500 wavenumbers are typical from common functional groups, for example, $-\text{OH}$, $\text{C}=\text{O}$, $\text{N}-\text{H}$, and CH_3 . The region between 1500-400 wavenumbers is often referred to as the fingerprint region. Absorption bands in this region are generally due to intra-molecular phenomena and are highly material specific. The specificity of these bands allow computerized data searches to be performed against reference libraries to identify a material. FTIR can be used to identify the chemical structure of almost any polymer and is perhaps the most powerful tool for identifying types of chemical bonds (functional groups).

An exemplar FTIR spectrum is shown in [Figure 2.62](#). This figure shows both the measured spectrum and the best library spectrum that was found by the FTIR software to match the experimentally determined results.

2.6.2 Energy Dispersive Spectroscopy

Energy dispersive X-ray spectroscopy (EDS) is a chemical microanalysis technique that, as was discussed in [Section 2.4.2](#), is typically performed in conjunction with an SEM. The EDS technique utilizes X-rays that are emitted from the sample during bombardment by the electron beam to characterize the elemental composition of the analyzed volume on a micro- or nano-scale.

In an SEM, an electron beam is scanned across the sample surface and generates X-ray fluorescence from the atoms in its path. The energies of the X-ray photons are characteristic of the element which produced it. The EDS X-ray detector measures the number of emitted X-rays versus their energy. The energy of the X-ray is characteristic of the chemical element from which the X-ray was emitted.

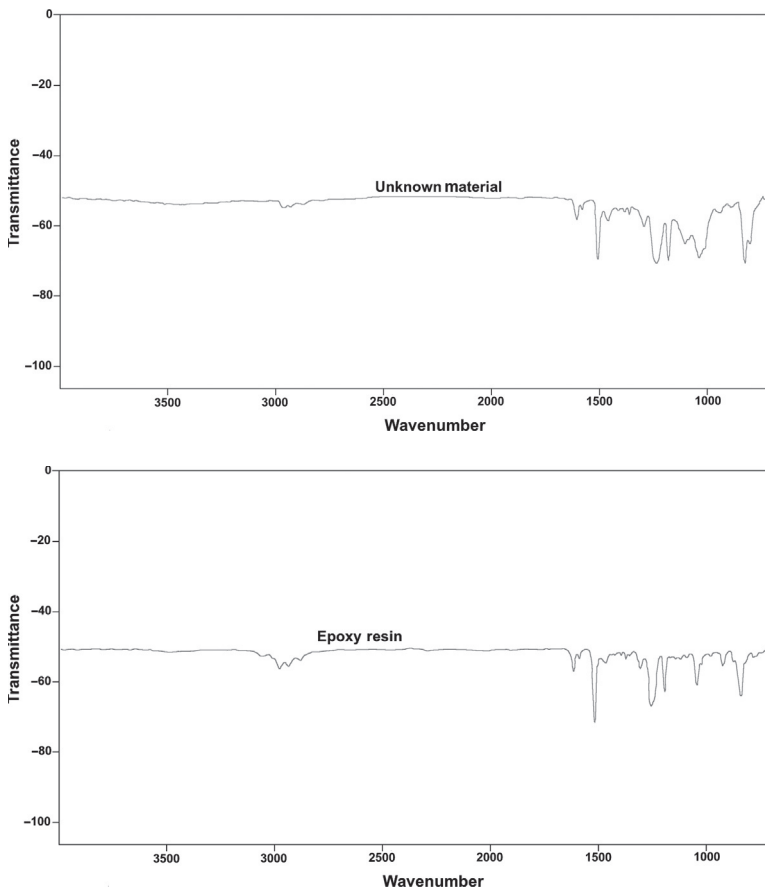


Figure 2.62 Exemplar FTIR spectrum from an unknown material, and the best matching library spectrum.

By determining the energies of the X-rays emitted from the area being excited by the electron beam, the elements present in the sample can be determined. This mode of operation is called qualitative analysis since only the types of elements in the sample are determined. The rate of detection of these characteristic X-rays can also be used to measure the amounts of elements present. This mode is called quantitative analysis. If the electron beam is swept over an area of the sample, then the EDS systems can also acquire X-ray maps showing spatial variation of elements in the sample.

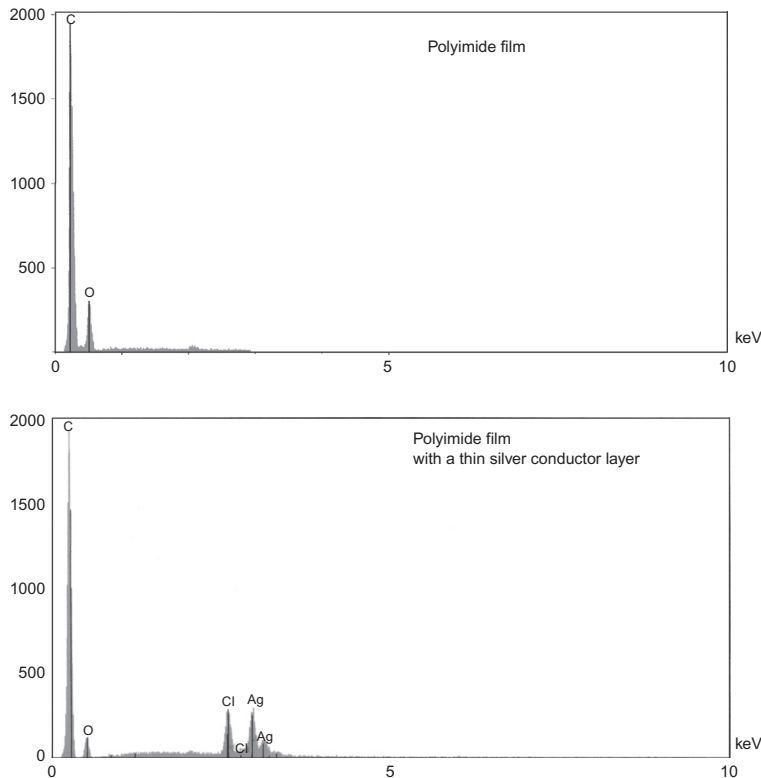


Figure 2.63 (a) EDS spectrum of a pure polyimide film; (b) EDS spectrum of polyimide film with a thin silver conductor layer.

An exemplar EDS spectrum is shown in Figure 2.63. This figure shows the spectrum for a polyimide film that is covered with a thin silver conductor layer. As indicated in the figure the EDS system only provides information about the chemical elements present in the sample, and do not specify the molecular structure.

Typical applications of EDS are in materials research, quality control, failure analysis, and forensic science.

2.6.3 Size-Exclusion Chromatography

Size-exclusion chromatography (SEC), also known as gel permeation chromatography (GPC), is a chromatographic method in

which molecules are separated based on their size. This method is most widely used in the analysis of polymer molecular weights (or molar mass).

In SEC, a column typically made of steel with a diameter of 10 mm and a length of 500-1000 mm, is packed with a porous material (typically silica or crosslinked polystyrene) and solvent is forced through the column at rates typically 1 ml/min and pressures of 50-200 bar. A sample is dissolved in the same solvent that is running through the column and is then introduced into the solvent stream going through the column. A detector monitors the concentration of sample exiting the end of the column. Inside the column, molecules are separated based on their hydrodynamic volume (the volume the molecule occupies in a dilute solution). For polymers this can vary greatly with the particular solvent and the temperature. By studying the properties of polymers in particular solvents and by calibrating each column setup with samples of known molecular weight, it is possible to get a relative distribution of molecular weights for a given polymer sample. Using this data, it is possible to calculate number-average molecular weight, weight-average molecular weight, polydispersity, as well as higher order molecular weights to within a useful level of accuracy.

Inside the column, molecules are separated by whether or not they can fit within the pore size of the packing material. When columns are created they are packed with porous beads with a specific pore size so that they are most accurate at separating molecules with sizes similar to the pore size. As a molecule flows through the column it passes by a number of these porous beads. If the molecule can fit inside the pore then it is drawn in by the force of diffusion. There it stays a short while and then moves on. If a molecule cannot fit into a pore then it continues following the solvent flow. For this reason, in an SEC column, molecules with larger size will reach the end of the column before molecules with smaller size. The effective range of the column is determined by the pore size of the packing. Any molecules larger than all the pores in a column will be eluted together regardless of their size. Likewise, any molecules that can fit into all the pores in the packing material will elute at the same time.

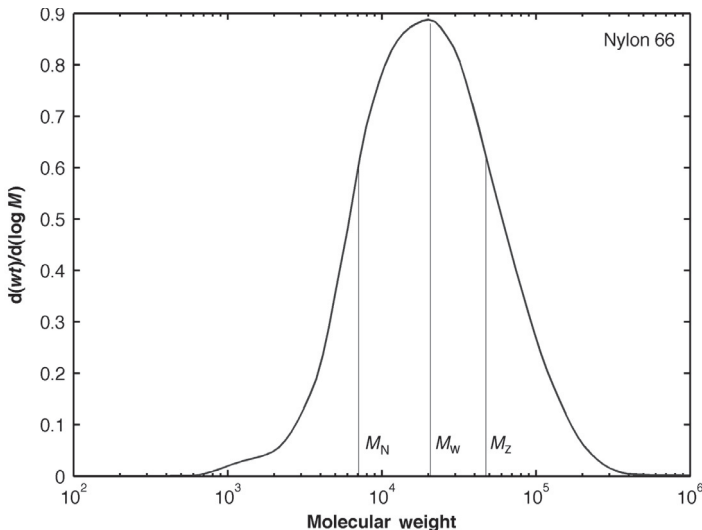


Figure 2.64 SEC results for a Nylon 66 showing the definition of M_N , M_W , and M_Z .

It is important to remember that the only absolute measure in SEC is volume of the molecule (hydrodynamic volume), and even that measurement has certain error built into it. Interactions between the solvent, packing, and or the sample will affect the measurement as will concentration due to sample-sample interactions. Calculating the molecular weight from this molecular size introduces even more error into the system. SEC is a useful tool for determining molecular weight in polymers, but it is essential that the column and instrumentation be carefully equilibrated and properly calibrated for the results to be trusted.

The molecular weight of a polymer is typically continuously distributed over a certain range, see Figure 2.64. Three different scalar quantities are commonly used to describe the molecular weight distribution:

1. *The number average* (arithmetic mean) molecular weight, M_N , is defined by

$$M_N = \sum_i \left\{ \frac{N_i}{\sum_j N_j} \right\} M_i = \frac{\sum_i N_i M_i}{\sum_j N_j}. \quad (2.16)$$

The number average is sensitive to small molecules.

2. *The weight average* molecular weight, M_W , is defined by

$$M_W = \sum_i \left\{ \frac{N_i M_i}{\sum_j N_j M_j} \right\} M_i = \frac{\sum_i N_i M_i^2}{\sum_j N_j M_j} = \frac{\sum_i w_i M_i}{\sum_j w_j}, \quad (2.17)$$

where w_i is the weight fraction of molecule i . The weight average molecular weight is more sensitive to heavy molecules.

3. *The Z-averaged* molecular weight, M_Z , is defined by

$$M_Z = \frac{\sum_i N_i M_i^3}{\sum_j N_j M_j^2}. \quad (2.18)$$

It is important to realize that the weight-averaged molecular weight is larger than or equal to the number average molecular weight: $M_W \geq M_N$. The ratio of the weight-average and number-average molecular weight is referred to as the polydispersity index:

$$PDI = \frac{M_W}{M_N}, \quad (2.19)$$

and is a measure of how widely distributed the molecular weight distribution is.

The mechanical properties of a polymeric material is often strongly dependent on the molecular weight of the material. [Figure 2.65](#) shows the results from an SEC investigation of two Nylon 66 specimens. One of the specimens had been exposed to chlorinated water for an extended amount of time. This specimen was heavily discolored and contained a large amount of surface cracks. The other specimen had only been exposed to chlorinated water for a short amount of time. As is shown in [Figure 2.65](#), the molecular weight of the Nylon 66 material is decreasing with

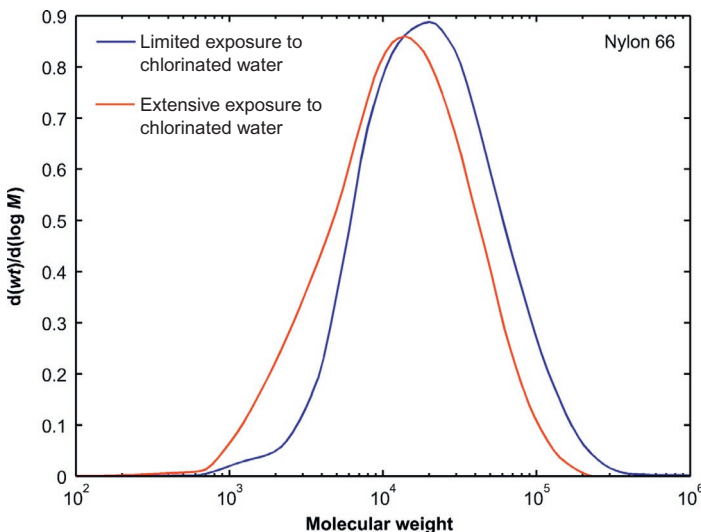


Figure 2.65 SEC results for two Nylon 66 samples exposed to different amounts of chlorinated water.

exposure time to chlorinated water and the polydispersity of the material is also increased.

2.6.4 Thermogravimetric Analysis

Thermogravimetric analysis (TGA) is a thermal analysis technique that can measure changes in the weight (mass) of a sample as a function of temperature and time. TGA is commonly used to determine polymer degradation temperatures, residual solvent levels, absorbed moisture content, and the amount of inorganic (noncombustible) filler in polymer or composite material compositions.

In slightly simplified terms, in TGA a sample is placed into a tared TGA sample pan which is attached to a sensitive microbalance device. The sample holder portion is subsequently placed into a high temperature furnace. The balance device measures the initial sample weight at room temperature and changes in sample weight as heat is applied to the sample. TGA tests can be run either in heating mode at a controlled heating rate, or isothermally.

Typical weight loss profiles can then be analyzed for the amount or percent of weight loss at any given temperature, the amount or percent of noncombusted residue at some final temperature, and the temperatures of various sample degradation processes.

Various atmospheres can be used to investigate sample reactions. Furthermore, TGA can be coupled with infrared spectroscopy (TGA/FTIR) to identify the evolved gases.

Typical applications of TGA include:

- weight loss/gain;
- drying rate;
- reactivity with atmospheres;
- oxidative degradation;
- reaction kinetics;
- volatilization analysis;
- compound composition; and
- stabilizer effectiveness.

As an example of the use of TGA is shown in [Figure 2.66](#), two TGA scans of silicone rubber. The first scan is for an unfilled silicon rubber and the second scan is for a silicone rubber with

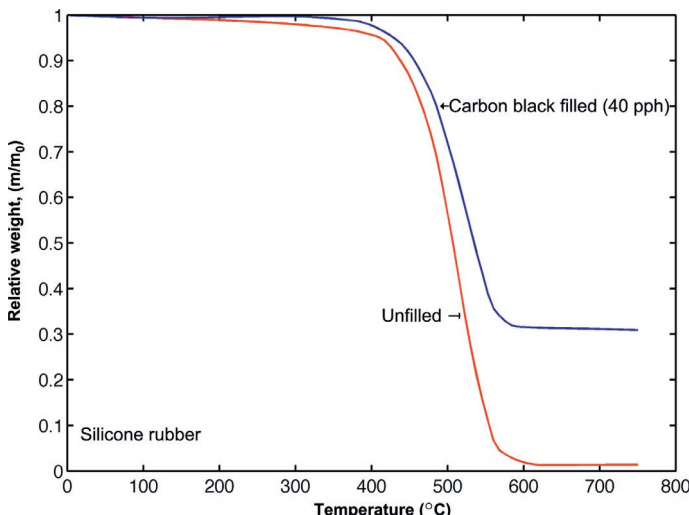


Figure 2.66 TGA scans of two silicon rubbers.

40 pph carbon black. The figure shows that the highly filled rubber start to degrade at a higher temperature than the unfilled rubber.

2.6.5 Raman Spectroscopy

Raman spectroscopy is a spectroscopic technique used to study vibrational, rotational, and other low-frequency modes in a material system. It relies on inelastic scattering, or Raman scattering of monochromatic light, usually from a laser in the visible, near infrared, or near ultraviolet range. Phonons or other excitations in the system are absorbed or emitted by the laser light, resulting in the energy of the laser photons being shifted up or down. The shift in energy gives information about the phonon modes in the system. Infrared spectroscopy yields similar, but complementary information.

When light is scattered from a molecule, most photons are elastically scattered. The scattered photons have the same energy (frequency) and, therefore, wavelength, as the incident photons. However, a small fraction of light (approximately 1 in 10^7 photons) is scattered at optical frequencies different from, and usually lower than, the frequency of the incident photons. The process leading to this inelastic scatter is called the Raman effect. Raman scattering can occur with a change in vibrational, rotational, or electronic energy of a molecule. Polymer chemists are concerned primarily with the vibrational Raman effect. In the following, we will use the term Raman effect to mean vibrational Raman effect only.

The difference in energy between the incident photon and the Raman scattered photon is equal to the energy of a vibration of the scattering molecule. A plot of intensity of scattered light versus energy difference is called a Raman spectrum.

In Raman spectroscopy, a laser beam is used to irradiate a spot on the sample under investigation. The scattered radiation produced by the Raman effect contains information about the energies of molecular vibrations and rotations, and these depend on the particular atoms or ions that comprise the molecule, the chemical bonds that connect them, the symmetry of their

molecule structure, and the physico-chemical environment where they reside.

Typically, a sample is illuminated with a laser beam. Light from the illuminated spot is collected with a lens and sent through a monochromator. Wavelengths close to the laser line (due to elastic Rayleigh scattering) are filtered out and those in a certain spectral window away from the laser line are dispersed onto a detector.

Spontaneous Raman scattering is typically very weak, and as a result the main difficulty of Raman spectroscopy is separating the weak inelastically scattered light from the intense Rayleigh scattered laser light. Raman spectrometers typically use holographic diffraction gratings and multiple dispersion stages to achieve a high degree of laser rejection. A photon-counting photomultiplier tube (PMT) or, more commonly, a CCD camera is used to detect the Raman scattered light.

Raman spectroscopy is commonly used for polymers, since vibrational information is very specific for the chemical bonds in molecules. It therefore provides a fingerprint by which the molecule can be identified.

2.7 Exercises

1. Does a semicrystalline polymer have a glass transition temperature? Why/why not?
2. How does the Young's modulus change with temperature for an amorphous polymer? For a semi-crystalline polymer?
3. What is Mullins effect? What type of polymer exhibit the strongest Mullins effect?
4. What are the most common ways to reduce the influence of friction in a uniaxial compression test?
5. Does all polymers neck when pulled in tension? Why/why not?
6. What are some common mechanical tests that are performed on polymers to determine the mechanical behavior?

7. What tests would you recommend in order to get experimental data for calibrating a viscoplastic material model?
8. What is the difference between the Sharpy and Izod impact tests?
9. What are the strengths and weaknesses of the DMA testing?
10. What are the two most common hardness tests that are performed on polymers?
11. What cannot SHPB testing be performed on soft polymers?
12. When is it necessary to perform bulk modulus testing on a polymer?
13. What are some of the most common experimental techniques for determining the failure behavior of a polymer?
14. What is the difference between verification and validation?
15. What experimental tests would you perform in order to validate an already calibrated material model?
16. List a few common techniques that can be used to study the surface characteristics of a polymer sample.
17. How does the DSC technique work? What data can be obtained from a DSC experiment?
18. Is SEM or TEM more commonly used for polymer mechanics analysis? Why?
19. What is the Bragg law and How is used in X-ray diffraction experiments?
20. Explain how birefringence can be used to aid the development of a hyperelastic material model for a rubber.
21. What are two techniques that can be used to determine the molecular weight of a polymer sample?
22. What are the definitions of number-average, weight-average, and z-average molecular weight?
23. What information can be obtained from an FTIR experiment?
24. Explain a situation when it might be useful to perform a TGA experiment.

References

- [1] ASTM D575, Standard Test Methods for Rubber Properties in Compression, 2001.
- [2] M.C. Boyce, K. Kear, S. Socrate, K. Shaw, Deformation of thermoplastic vulcanizates, *J. Mech. Phys. Solids*, 49 (2001) 1073-1098.
- [3] J.S. Bergström, M.C. Boyce, Constitutive modeling of the large strain time-dependent behavior of elastomers, *J. Mech. Phys. Solids*, 46 (1998) 931-954.
- [4] ASTM D2990, Standard Test Methods for Tensile, Compressive, and Flexural Creep and Creep-Rupture of Plastics, 2001.
- [5] ASTM D412, Standard Test Methods for Vulcanized Rubber and Thermoplastic Elastomers—Tension, 2002.
- [6] ASTM D638, Standard Test Method for Tensile Properties of Plastics, 2003.
- [7] ASTM D256, Standard Test Methods for Determining the Izod Pendulum Impact Resistance of Plastics, 2004.
- [8] ASTM D6110, Standard Test Method for Determining the Charpy Impact Resistance of Notched Specimens of Plastics, 2004.
- [9] ISO 179, Plastics—Determination of Charpy Impact Properties—Part 1: Non-Instrumented Impact Test, 2000.
- [10] ISO 180, Plastics—Determination of Izod Impact Strength, 2000.
- [11] ASTM D5420, Standard Test Method for Impact Resistance of Flat, Rigid Plastic Specimens by Means of a Striker Impacted by a Falling Weight (Gardner Impact), 2004.
- [12] ASTM D1709, Standard Test Methods for Impact Resistance of Plastic Films by the Free-Falling Dart Method, 2004.
- [13] Veryst Engineering, Instrumented Impact Testing. Available from: <http://www.veryst.com/what-we-offer/material-testing-modeling>.
- [14] J.D. Ferry, Viscoelastic Properties of Polymers, John Wiley & Sons, Inc., New York, 1980.
- [15] K. Menard, Dynamic Mechanical Analysis: A Practical Introduction, CRC Press, Boca Raton, FL, 1999.
- [16] ASTM D4065, Standard Practice for Plastics: Dynamic Mechanical Properties: Determination and Report of Procedures, 2001.
- [17] ISO 6721, Plastics—Determination of Dynamic Mechanical Properties, 1994.
- [18] ASTM D785, Standard Test Method for Rockwell Hardness of Plastics and Electrical Insulating Materials, 2003.

- [19] ASTM D2240, Standard Test Method for Rubber Property—Durometer Hardness, 2004.
- [20] ASTM D2583, Standard Test Method for Indentation Hardness of Rigid Plastics by Means of a Barcol Impressor, 2001.
- [21] W.W. Chen, B. Song, Split Hopkinson (Kolsky) Bar: Design, Testing, and Applications, Springer, New York, 2010.
- [22] D. Walsh, P. Zoller, Standard Pressure Volume Temperature Data for Polymers, CRC Press, Boca Raton, FL, 1995.
- [23] W. Young, R. Budynas, A. Sadegh, Roark's Formulas for Stress and Strain, McGraw-Hill Professional, New York, 2011.
- [24] ASTM D0624, Standard Test Method for Tear Strength of Conventional Vulcanized Rubber and Thermoplastic Elastomers, 2012.
- [25] ASTM D6068, Standard Test Method for Determining J-R Curves of Plastic Materials, 2010.
- [26] ASTM F2183, Standard Test Method for Small Punch Testing of Ultra-High Molecular Weight Polyethylene Used in Surgical Implants, 2002.
- [27] J.S. Bergström, C.M. Rimnac, S.M. Kurtz, Prediction of multiaxial mechanical behavior for conventional and highly crosslinked UHMWPE using a hybrid constitutive model, *Biomaterials*, 24 (2003) 1365-1380.
- [28] J.S. Bergström, C.M. Rimnac, S.M. Kurtz, Molecular chain stretch is a multiaxial failure criterion for conventional and highly crosslinked UHMWPE, *J. Orthop. Res.*, 23 (2003) 367-375.
- [29] J.S. Bergström, C.M. Rimnac, S.M. Kurtz, An augmented hybrid constitutive model for simulation of unloading and cyclic loading behavior of conventional and highly crosslinked UHMWPE, *Biomaterials*, 25 (2004) 2171-2178.
- [30] ASTM D5379, Standard Test Method for Shear Properties of Composite Materials by the V-Notch Beam Method, 2012.
- [31] R.J. Cherry, New Techniques of Optical Microscopy and Microspectroscopy, CRC Press, Boca Raton, FL, 1991.
- [32] B. Herman, J.J. Lemasters, Optical Microscopy: Emerging Methods and Applications, Academic Press, San Diego, CA, 1992.
- [33] G. Binnig, C.F. Quate, Ch. Geber, Atomic Force Microscope, *Phys. Rev. Letters* (1986) 930.
- [34] O.A. Hasan, M.C. Boyce, Energy storage during inelastic deformation of glassy polymers, *Polymer*, 34 (24) (1993) 5085-5092.
- [35] J.S. Bergström, Large strain time-dependent behavior of elastomeric materials, Ph.D. thesis, MIT 1999.

- [36] R.A. Pethrick, C. Viney, X-ray diffraction from crystalline polymers, in: Experimental Methods in Polymer Characterisation, John Wiley & Sons, Sussex, 2003.
- [37] R.W. Richards, Wide angle X-ray scattering, in: Scattering Methods in Polymer Science, Ellis Horwood, London, 1995
- [38] H.P. Klug, L.E. Alexander, X-Ray Diffraction Procedures: For Polycrystalline and Amorphous Materials, second ed., Wiley-Interscience, New York, 1974.
- [39] G.H. Meeten, Optical Properties of Polymers, Elsevier, New York, 1986.
- [40] ASTM D2765, Standard Test Method for Determination of Gel Content and Swell Ratio of Crosslinked Ethylene Plastics, 2001.
- [41] ASTM F2214, Standard Test Method for In Situ Determination of Network Parameters of Crosslinked Ultra High Molecular Weight Polyethylene (UHMWPE), 2002.
- [42] P.J. Flory, Principles of Polymer Chemistry, Cornell University Press, Ithaca, NY, 1953.